NUWC-NPT Technical Report 11,415
14 February 2003

Mechanics of Pressurized Plain-Woven Fabric Structures

Paul V. Cavallaro
Matthew E. Johnson
NUWC Division Newport

Ali M. Sadegh
The City College of the City University, New York

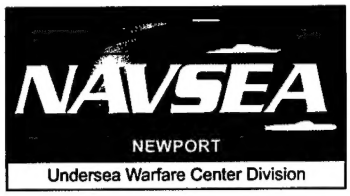

Naval Undersea Warfare Center Division
Newport, Rhode Island

PREFACE

This research was conducted in support of the Center of Excellence for Inflatable Composite Structures at the U.S. Army Soldier Biological Chemical Command (SBCCOM) in Natick, MA, through Military Interagency Purchase Request Number 2HS6R00650, NUWC Assignment Number TD0207. The SBCCOM project officer is Jean Hampel.

The technical reviewer for this report was Anthony J. Kalinowski (Code 74).

The authors wish to give special thanks to Jean Hampel and Jack Siegel of SBCCOM for sponsoring this effort. Also, invaluable assistance was received from Federal Fabrics-Fibers Inc. of Lowell, MA, which manufactured the woven air beams, and, in particular, from founder Zvi Horovitz and senior engineer Fred Guerts, who participated in informative discussions on the details of the weaving process. Finally, sincere appreciation is extended to Martin Leff (NUWC Code 72) for providing experimental test support and Anthony J. Kalinowski (NUWC Code 74) for his careful review of the manuscript.

Reviewed and Approved: 14 February 2003

Thomas A. Casey
Head, Engineering, Test & Evaluation Department

REPORT DOCUMENTATION PAGE

Form Approved
OMB No. 0704-0188

1. AGENCY USE ONLY *(Leave blank)*	2. REPORT DATE	3. REPORT TYPE AND DATES COVERED
	14 February 2003	

4. TITLE AND SUBTITLE

Mechanics of Pressurized Plain-Woven Fabric Structures

5. FUNDING NUMBERS

6. AUTHOR(S)

Paul V. Cavallaro
Matthew E. Johnson
Ali M. Sadegh

7. PERFORMING ORGANIZATION NAME(S) AND ADDRESS(ES)

Naval Undersea Warfare Center Division
1176 Howell Street
Newport, RI 02841-1708

8. PERFORMING ORGANIZATION REPORT NUMBER

TR 11,415

9. SPONSORING/MONITORING AGENCY NAME(S) AND ADDRESS(ES)

U.S. Army Soldier Biological Chemical Command
Kansas Street
Natick, MA 01760

10. SPONSORING/MONITORING AGENCY REPORT NUMBER

11. SUPPLEMENTARY NOTES

12a. DISTRIBUTION/AVAILABILITY STATEMENT

Approved for public release; distribution is unlimited.

12b. DISTRIBUTION CODE

13. ABSTRACT (Maximum 200 words)

Pressurized fabric tubes, pressure-stabilized beams (known as air beams), and air-inflated structures are all considered to be valuable technologies for use in lightweight, rapidly deployable systems. The design optimization of inflated structures, in particular, depends on a thorough understanding of woven-fabric mechanics. With this in mind, the bending response of woven pressure-stabilized beams were experimentally tested and analytically investigated. Additionally, the micromechanical effects of interacting tows were examined through the use of finite-element models containing contact surfaces and nonlinear slip/stick conditions. Local unit-cell models consisting of pairs of woven tows were created to characterize the effective constitutive relations. Material properties from the unit-cell models were then used with a global continuum model subjected to four-point flexure. An experimental setup was designed and manufactured for the testing of Vectran and polyethylene naphthalate air beams, with mid-span beam deflections measured as functions of inflation pressure and bending load. Plots of the elastic and shear moduli with respect to the pressure and coefficient of friction were generated. It was determined that the effective elastic and shear moduli were functions of inflation pressure, the material in use, and the geometry of the weave. It was further shown that pneumatic or pressurized fabric structures differ fundamentally from conventional metallic structures.

14. SUBJECT TERMS

Woven-Fabric Mechanics; Pressurized Fabric Structure; Interacting Woven Tows; Textile Engineering; Air Beams; Inflated Tensile Structures; Pressure Stabilized Beams

15. NUMBER OF PAGES
46

16. PRICE CODE

17. SECURITY CLASSIFICATION OF REPORT	18. SECURITY CLASSIFICATION OF THIS PAGE	19. SECURITY CLASSIFICATION OF ABSTRACT	20. LIMITATION OF ABSTRACT
Unclassified	Unclassified	Unclassified	SAR

TABLE OF CONTENTS

	Page
LIST OF TABLES	ii
INTRODUCTION	1
LITERATURE REVIEW	3
EXPERIMENTS	5
ANALYTICAL STRAIN-ENERGY SOLUTION	13
UNIT-CELL MODELS	15
Shell Unit-Cell Model	17
Beam-Element Unit-Cell Model	21
Finite-Element Model	26
RESULTS	27
CONCLUSIONS	32
REFERENCES	35

LIST OF ILLUSTRATIONS

Figure		Page
1	Experimental Fixture for Four-Point-Bend Tests	6
2	Enlarged View of Single Vectran Tow	7
3	Four-Point-Bend Load-Deflection Curves for 50.8 mm (2.0-Inch) Diameter Vectran Air Beam at Constant Pressure	8
4	Four-Point-Bend Load-Deflection Curves for Vectran Air Beam at Constant Pressures of 0.138 MPa (20 psi), 0.207 MPa (30 psi), and 0.276 MPa (40 psi) Showing Load-Rate Dependence	9
5	Four-Point-Bend Load-Deflection Curves for Coated and Uncoated Vectran Air Beams at Constant Pressure of 0.138 MPa (20 psi)	9
6	Four-Point-Bend Load-Deflection Curves for Vectran Air Beam at Constant Pressures of 0.138 MPa (20 psi) and 0.207 MPa (30 psi) Using Wide-Span Setup	11
7	Stages of Fabric Air Beam Deformations	11

LIST OF ILLUSTRATIONS (Cont'd)

Figure		Page
8	Comparison of Vectran and PEN Air Beams Subjected to Wide-Span, Four-Point Bending	12
9	Tensile Tests of Vectran and PEN Tows	12
10	Four-Point-Bend Parameters for Analytical Strain-Energy Solution	15
11	Kinematic Tow Interaction Modeling Methods	16
12	Pressure Application Options for Shell Unit-Cell Model	18
13	Shell Unit-Cell Model	19
14	Hypothesized Bladder/Tow Interaction for Large-Weave Spacing	22
15	Tow Necking in Beam-Element Model	22
16	Orthogonal Beam-Element Tow Interaction Model	23
17	Beam-Element Unit-Cell Model	24
18	Rate-Dependent Elastic Modulus of As-Woven Vectran Warp and Weft Tows	29
19	Nondimensionalized Plot of Fabric Modulus (E_1) Versus Pressure for Various Coefficients of Friction	30
20	Nondimensionalized Plot of Fabric Modulus (E_2) Versus Pressure for Various Coefficients of Friction	30
21	Nondimensionalized Plot of Fabric Shear Modulus($G_f = G_{12}$) Versus Pressure for Various Coefficients of Friction	31
22	Contour Plot of Shear Stress (τ_{12}) for Quarter-Symmetry, Four-Point-Bend Finite-Element Model	31
23	Comparison of Results from Four-Point-Bend Finite-Element Shell Model to Experimental Results for 50.8-mm (2.0-Inch) Diameter Vectran Air Beam at 0.138 MPa (20 psi)	32

LIST OF TABLES

Table		Page
1	Tensile Properties of As-Woven Vectran and PEN Tows	28

MECHANICS OF PRESSURIZED PLAIN-WOVEN FABRIC STRUCTURES

INTRODUCTION

In the past three decades, plain-woven fabrics have been utilized as materials in air-inflated, rapidly deployable structures (including temporary shelters and bridges, tents, and space systems). Unlike metallic structures, air-inflated structures are primarily designed to be light-weight, have deployed-to-stowed volume ratios that can be on the order of 1000 to 1, and may even be self-erecting. Pressurized fabric tubes and pressure-stabilized beams (known as air beams) are typically used as the basic load-carrying members of these structures.

Although available for many years, such valuable technologies have not yet been refined to the extent that reliable structures can be analytically designed. With the advent of fiber materials and weaving/braiding technologies that have improved the load-carrying capacity of pressurized fabric structures, an increasing interest has developed in the modeling of mechanical behavior for woven fabrics. However, this class of composite materials has complex microstructures that lead to complicated mechanical responses. In particular, the mechanical characteristics of plain-woven fabrics used in inflated structures, unlike traditional composite materials, exhibit high nonlinearity, with dependence on the internal pressure and contact interactions within the woven fabric.

Inflated structures generally consist of woven yarns or tows made from plastic, Kevlar, polyethylene naphthalate (PEN), thermoplastic liquid crystal polymer (Vectran), polymer, or textile fibers, along with an internal bladder. The bladder is intentionally compliant and may be filled with air, water, gel, or sand to create internal pressure. Such pressure is equilibrated by the reaction forces exerted from the tows. Once the tows are sufficiently stressed, an inflated structure acquires a flexural stiffness that is capable of resisting bending loads.

The woven fabrics are formed by interlacing warp and weft tows. The direction of weaving is called the warp (axial) direction, and the normal direction is called the weft (hoop), or fill, direction. The weft tows alternately go over and under the warp tows (nearly orthogonally).

However, in braided fabrics, the warp and weft tows are not nearly orthogonal but, rather, are aligned with a bias angle to resist shearing loads. Straps of polymer fibers are attached to braided air beams to provide axial and bending stiffness.[1]

Woven air beams have axial and hoop stiffnesses that are only minimally coupled because of the nearly orthogonal placement of the warp and weft tows. That is, no tows are directly aligned to resist shearing deformations in these air beams. Rather, such deformations are resisted solely by rotational friction developed through pressure-induced contact among overlapping tows.

It remains impossible to model a complete assembly of air beam tows and their contact interfaces explicitly. This research has therefore developed constitutive relationships of the fabric materials that are based on capturing localized tow interaction effects from micro-mechanical unit-cell models. These relationships are then applied to a macromechanical continuum model to predict global flexural behavior as a function of inflation pressure and weave construction. The macromechanical models preserve the micromechanical influences on material behavior without subjecting the analysis to the computational penalties associated with an explicit modeling approach.

The primary goals of this investigation are to perform micromechanical and macro-mechanical modeling of air beams subjected to flexural loads and to characterize the effects of pressure, fabric materials, geometry, and the contact of interacting tows on the air beam response. The analysis method chosen here is designed to validate the following premises:

- The fabric elastic moduli are dependent upon pressure.
- The tow elastic modulus plays little role in the flexural stiffness of woven air beams at the operating pressures considered.
- The effects of the fabric transverse shearing deformations on global deflections of air beam are significant.
- The fabric shear stiffness is not a material property, but rather is a system property with dependence on pressure, weave density, and tow spacing.

LITERATURE REVIEW

During the 1960s and early 1970s, several investigations were performed on air beam structures during which the bending of pressurized cylindrical membranes or thin-walled cylindrical beams was addressed (see, for example, Stein and Hedgepeth,[2] Fichter,[3] and Bulson[4]). Because it was assumed in these studies that fabric compressive stresses were not admissible, the wrinkling moment was calculated as $\pi pr^3/2$, where p is the pressure and r is the mean radius. From the mid-1970s to the mid-1980s, in a series of technical reports, Steeves[5-9] documented the behavior of pressure-stabilized beams under load and linearized their deformation for the design of rib tents. Recently, because of the developments in fiber materials and braiding and weaving technologies, a whole host of new applications has emerged, attracting the attention of both the textile and engineering research communities.

The three clusters of literature on biaxially loaded woven fabrics include textile composite, structural composite, and inflated tensile structures, as described below:

- Textile composite publications generally address textile-forming techniques, knowledge of yarns and fibers, the strength of woven fabric in tension, or out-of-plane impact resistance. These documents do not consider inflation or pressurization as service loads, but rather regard the cross-section of the fabric as circular, elliptical, or rectangular with semicircular ends (racetrack). For example, Tarafaoui and Akesbi[10] developed a finite-element unit-cell model and simulated the tensile and pure shear tests of fabric. In another work, Bejan and Poterasu[11] described the woven fabric structure in detail and employed the basic stiffness tensor for orthotropic materials to determine the average stiffness and compliance matrices. Vandeurzen et al.[12] proposed a method of predicting the shear modulus for woven fabric composites.

- Structural composites — the second cluster of literature — examine in-plane effective elastic properties and the structural response of woven plain-fabric composites comprised of dense polymer fibers and a stiff matrix. There are many studies that provide an impact/damage analysis of laminated woven-fabric composites. For instance, Woo and Whitcomb[13] and Woo[14] developed a global/local finite-element

model for textile composites. Furthermore, Kuhn and Charalambides[15] and Kuhn et al.[16] presented a unit-cell geometry and addressed the modeling of a plain-woven fabric. In other efforts, Ruan and Chou[17] performed experimental and theoretical studies of the failure behavior of the knitted fabric composite, Hahn and Pandey[18] presented a micromechanical model to predict thermoelastic properties of plain-woven fabric composites, and Li et al.[19] analyzed two models, based on geometric modeling, to predict the fiber orientation of biaxially braided fabrics. Several articles in which the manufacture of woven fabrics are studied include those by Norman et al.,[20] Ueng and Cheng,[21] and Lim et al.[22] Dynamic failure of plain-woven fabrics is also an important behavior, and several studies have addressed high-velocity (Flanagan and Zikry[23]) and low-velocity (Siow and Shim[24]) impact failures of the fabric. The material properties of Vectran and PEN fibers are given in Warner.[25] The structural composites classification differs fundamentally from the present research in that the former category includes a matrix that binds the discrete tows together to minimize relative displacements and rotations.

- Inflated tensile structures — the third cluster of literature — examines the response of an inflated lightweight structure to service loads. Articles in this category generally assume homogeneous and isotropic material properties for the inflated structure and employ membrane or thin-shell theory to determine the structural response. This approach was introduced by Otto[26] in his book *Tensile Structures*. Plaut et al.[27] used linear thin-shell theory and formulated a governing equation for an arch, and Klute and Hannaford[28] developed a finite-element model and investigated pneumatic (artificial muscle) actuators.

In the reviewed literature, the effect of tow interactions due to pressurization of a woven fabric has not been addressed. In fact, most of the above-mentioned studies assumed the fabric to be a continuum and homogeneous material. In the study discussed here, however, the behavior of the warp and weft tows is assumed to be independent, which makes the fabric a noncontinuum and thus a load-dependent material. Furthermore, the tows of the fabric are treated independently, with the micromechanics of their interaction investigated.

EXPERIMENTS

As shown in the upper portion of figure 1, an experimental four-point-bending fixture was designed for use with an Instron machine to investigate the mechanical behavior of Vectran and PEN air beams. The upper and lower points are referred to as load and support points, respectively. Although Steeves[5] employed a three-point loading configuration, a four-point configuration was preferred in the present study for the following reasons. First, four-point bending generates a region of constant bending stress between load points where the transverse shear force is zero. Second, the applied load-point forces are one-half those found in the three-point bending arrangement, which reduces the possibility of initiating localized wrinkling or buckling in the vicinity of the load points.

Each point on the fixture was hinged to permit follower-type reactions, whereby the force vectors are allowed to rotate as the air beams deflect. Each point was also equipped with a semicircular saddle to eliminate potential knife-edge effects on the load transfer between the fixture and the air beams. The distance between support points was 1,127.125 mm (44.375 inches), and the distance between load points was 384.175 mm (15.125 inches). Therefore, by symmetry, the distance between a support and an adjacent load point was 371.475 mm (14.625 inches).

As shown in the lower portion of figure 1, a displacement wire transducer having a constant tension force of 1.390 N (5 ounces) was used to measure the mid-span deflection of the air beam. The internal pressure was monitored with a pressure gauge connected to the air valve attached to one end cap. Displacement-controlled loading was applied by the crosshead to the air beam at a constant rate, with the applied force measured directly from the Instron's load cell.

Air beams manufactured from plain-woven fabrics by Federal Fabrics-Fibers Inc. were used in the experiments. Six 243.8-cm (96.0-inch) long air beams were tested. Three were Vectran air beams with a 50.8-mm (2.0-inch) outer diameter (two of which were uncoated), and three were PEN air beams with a 50.8-mm (2.0-inch) outer diameter (two of which were uncoated). The warp and weft tows were near orthogonal and were made from 1,500-denier Vectran and PEN fibers with strengths (tenacity*) of 28 and 10 grams per denier (gpd), respectively. There

*The textile literature reports fiber strength as tenacity, which has units of grams per denier (gpd). Denier is defined as the mass in grams of a 9,000-m fiber of the tow.

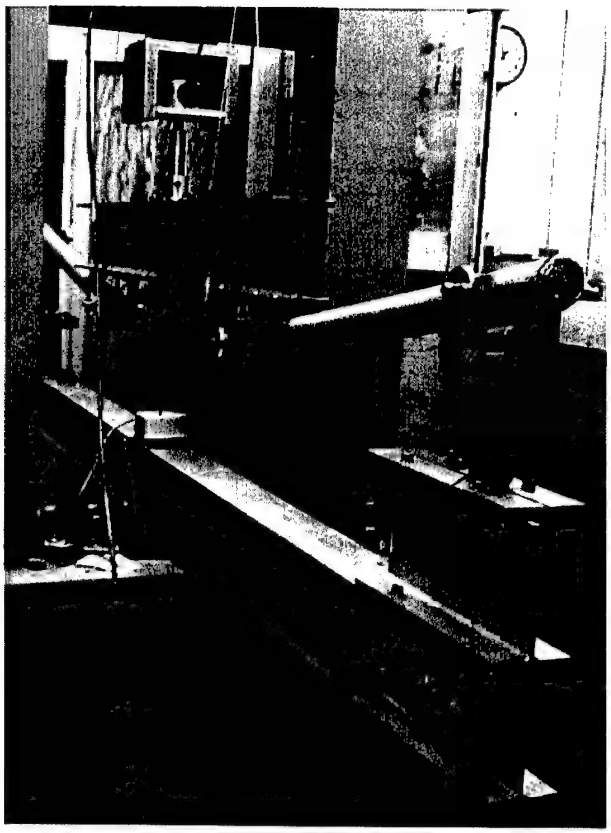

Overview of Experimental Fixture

Closeup of Displacement Wire Transducer for Mid-Span Deflection Measurement

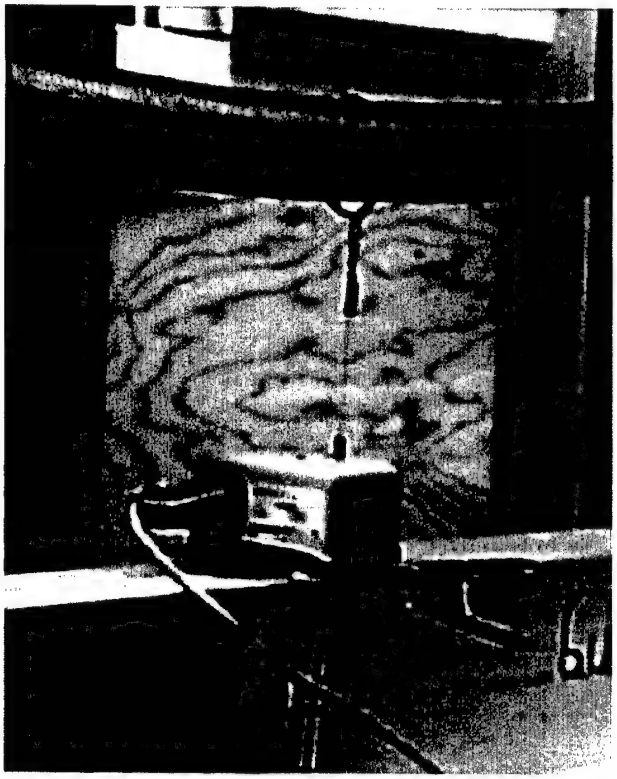

Figure 1. Experimental Fixture for Four-Point-Bend Tests

were 10 warps per inch of circumference and 19 wefts per inch of air beam length. End caps were stitched on the air beams, with one end cap equipped with an air valve. The bladder, made of Estane, had a thickness of 0.203 mm (0.008 inch). A microscopic examination of the fabric revealed that the warp and weft directional spacings were different, with the nominal spacing between adjacent warp tows at 1.20 mm and between adjacent weft tows at 0.10 mm. Figure 2, which shows an enlarged image of a single 1,500-denier Vectran tow, reveals that the tow is not a continuum but rather consists of 300 fibers (filaments), each with a diameter of 0.023 mm (9.06^{-4} inches).

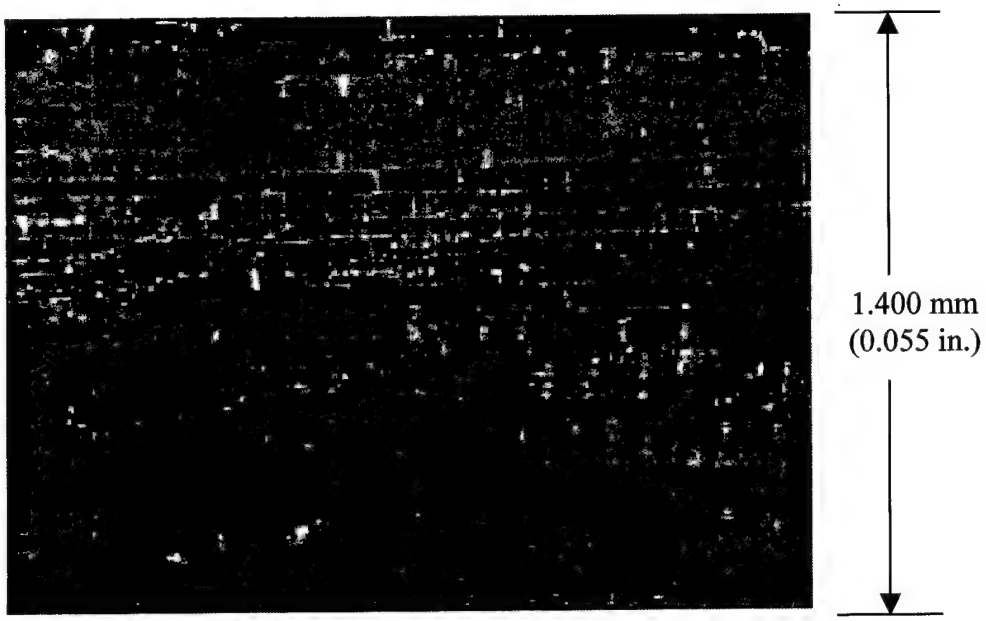

Figure 2. Enlarged View of Single Vectran Tow

The effect of pressure on the load-deflection behavior of a 50.8-mm (2.0-inch) diameter Vectran air beam was investigated. The air beam was initially pressurized to 0.138 MPa (20.0 psi) and then loaded until a mid-span deflection of 50.8 mm (2.0 inches) was achieved. The experiment was repeated for pressures up to 0.689-MPa (100-psi) by 0.0689-MPa (10-psi) increments. The load-versus-mid-span deflection curves for each pressure are shown in figure 3, where it is observed that the applied force increases with increasing pressure for a given mid-span deflection. That is, the flexural and shear stiffnesses increase as pressure increases.

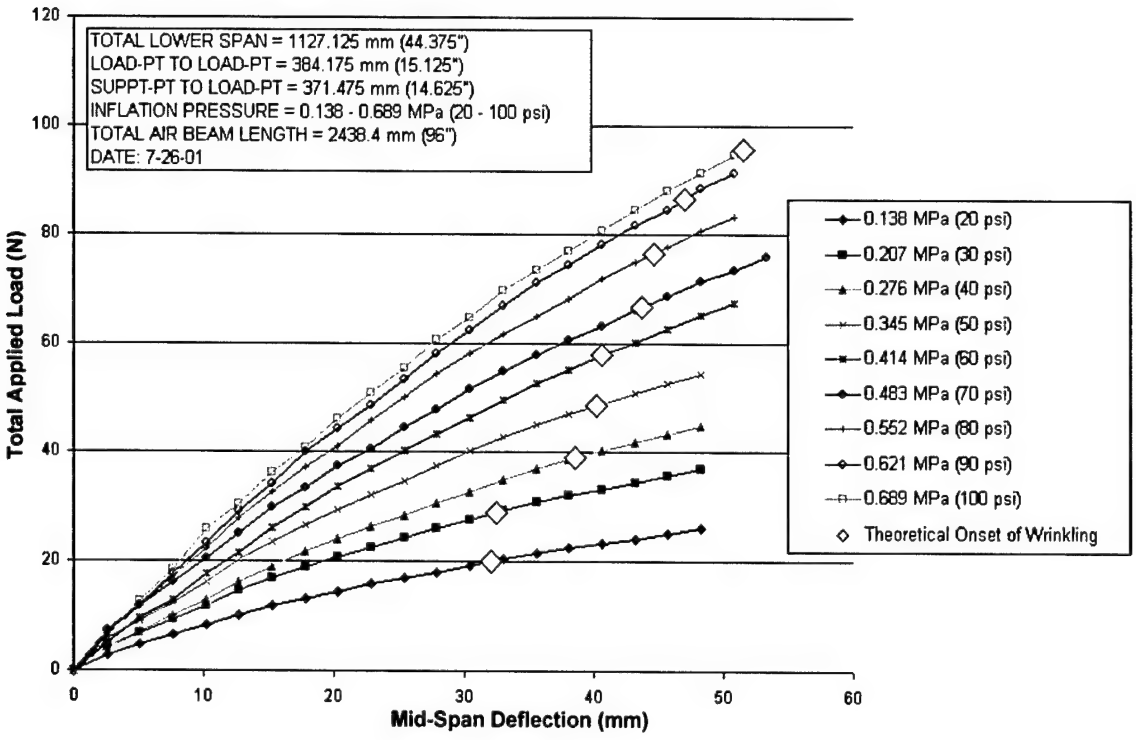

Figure 3. Four-Point-Bend Load-Deflection Curves for 50.8-mm (2.0-Inch) Diameter Vectran Air Beam at Constant Pressure

The effect of load rate on the flexural behavior of the 50.8-mm (2.0-inch) diameter Vectran air beam was investigated with the use of crosshead displacement rates of 12.7, 25.4, and 50.8 mm/minute (0.5, 1.0, and 2.0 inches/minute) at pressures of 0.138, 0.207, and 0.276 MPa (20, 30, and 40 psi), respectively. The mid-span deflections, measured as functions of pressure and displacement rates, are shown in figure 4.

Air beams are typically coated to minimize environmental degradation of the structural fibers. This coating reduces the relative motion (translations and rotations) of the warp and weft tows and thus increases the flexure and shear stiffness of the air beam. Such stiffening effects were investigated by subjecting a Vectran air beam coated with a neoprene/urethane layer to the four-point-bend test, with the load-deflection results of coated and uncoated Vectran air beams shown in figure 5. For a given deflection, the results indicate that the coated air beam requires twice the load of the uncoated air beam. Generally speaking, as the coating stiffnesses increase, the air beam becomes analogous to a matrix–based composite.

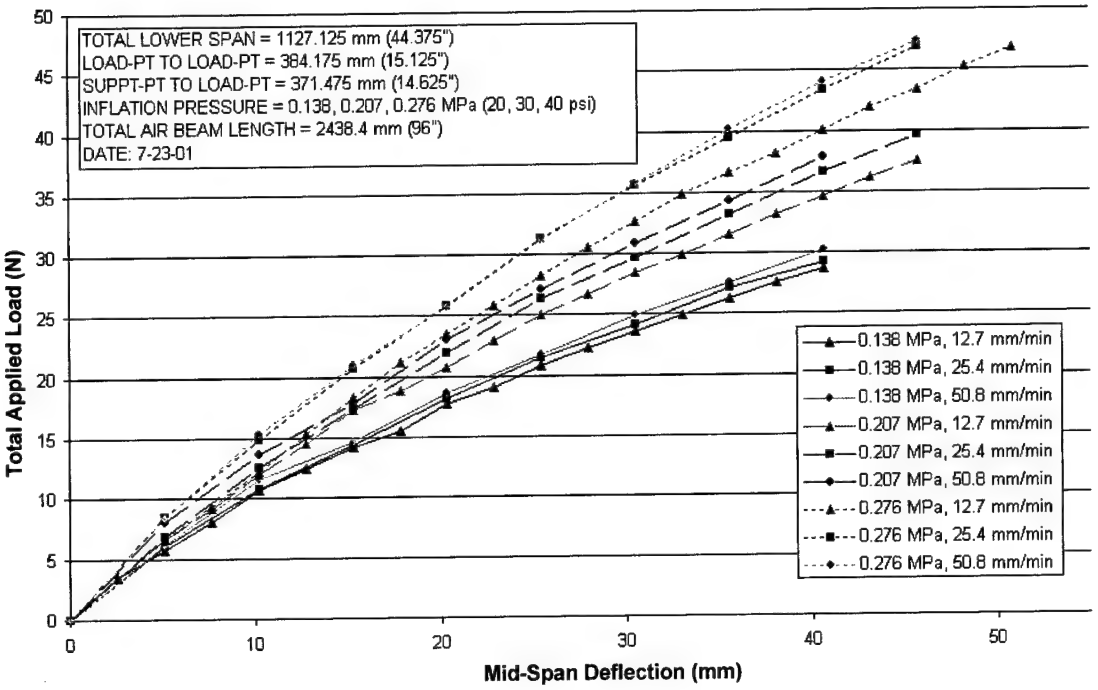

Figure 4. Four-Point-Bend Load-Deflection Curves for Vectran Air Beam at Constant Pressures of 0.138 MPa (20 psi), 0.207 MPa (30 psi), and 0.276 MPa (40 psi) Showing Load-Rate Dependence

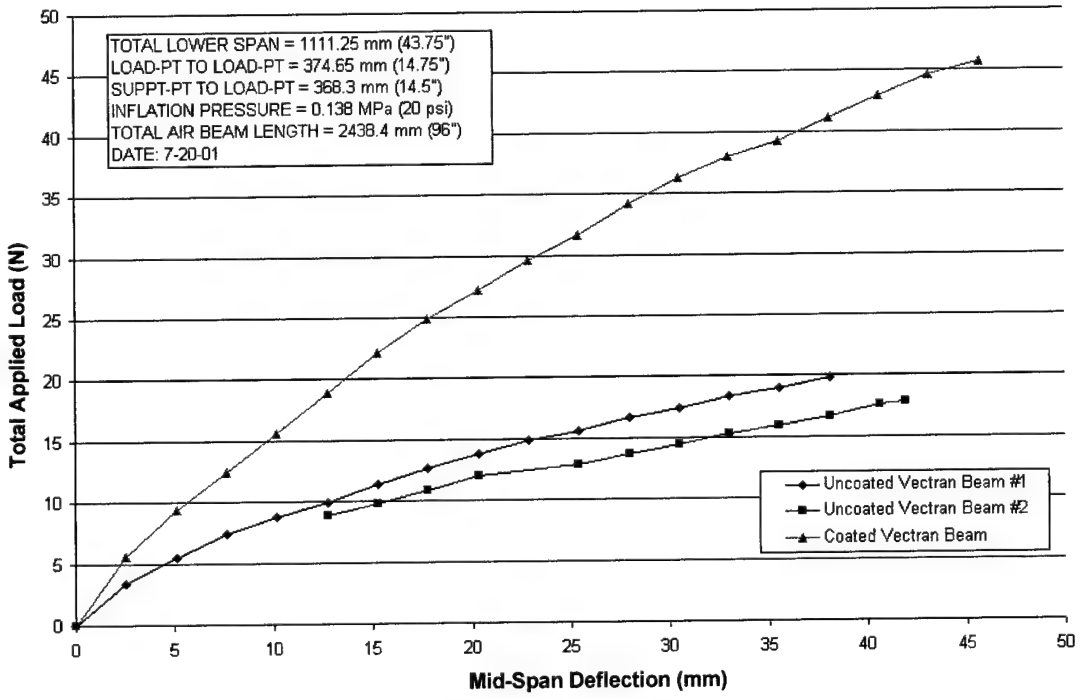

Figure 5. Four-Point-Bend Load-Deflection Curves for Coated and Uncoated Vectran Air Beams at Constant Pressure of 0.138 MPa (20 psi)

To allow further deflection of the air beam, the experimental setup was modified by nearly doubling the bending moment arm. That is, the distance between the supports and adjacent load points was increased to 685.8 mm (27.0 inches). With this approach, the mid-span deflection of the air beam was increased from 50.8 to 203.2 mm (2.0 to 8.0 inches); however, the maximum load was approximately 21.54 N (4.75 pounds) at an inflation pressure of 0.207 MPa (30 psi), as shown in figure 6.

All the above tests were repeated with two similar 50.8-mm (2.0-inch) diameter Vectran air beams. Although the air beams were from the same manufacturer, the load-deflection curves were not identical. The small difference between curves (only 5%) was attributed to the manufacturing tolerances observed during the weave process.

The angles between the warp and weft tows were examined before, during, and after the flexure experiments. Deformations of a 25.4- by 25.4-mm square region (located on the tensile surface at the mid span of the air beam) were monitored with a digital camera. Figure 7(a) depicts the woven tows at zero pressure. In this case, the angle between the two fibers is nearly 90°. Once pressurized, the angle between the tows remained at nearly 90° (as shown in figure 7(b)). However, when the air beam was subjected to bending loads, the average angle between the tows was changed by –3°, as shown in figure 7(c), indicating that the shear deformation is significant. Upon removal of the bending loads, the angle between tows returned to 90° (see figure 7(d)).

In the second set of experiments, the effect of pressure on the load-deflection curve of the 50.8-mm (2.0-inch) diameter PEN air beams was investigated. The air beam was 2,438.4 mm (96.0 inches) long and was used with the wide-span experimental setup (i.e., 835.025 mm (32.875 inches)). After the beam was inflated to 0.138 MPa (20 psi), the load-deflection curve was determined. The test was then repeated for a 0.207-MPa (30-psi) inflation pressure, resulting in the mid-span deflection seen in figure 8. The air beams were tested with internal pressures of 0.138 MPa (20 psi) and 0.207 MPa (30 psi) and with crosshead displacement rates of 12.7, 25.4, and 50.8 mm/minute (0.5, 1.0, and 2.0 inches/minute). The load-deflection curves of PEN air beams as compared to those of Vectran air beams are shown in the figure.

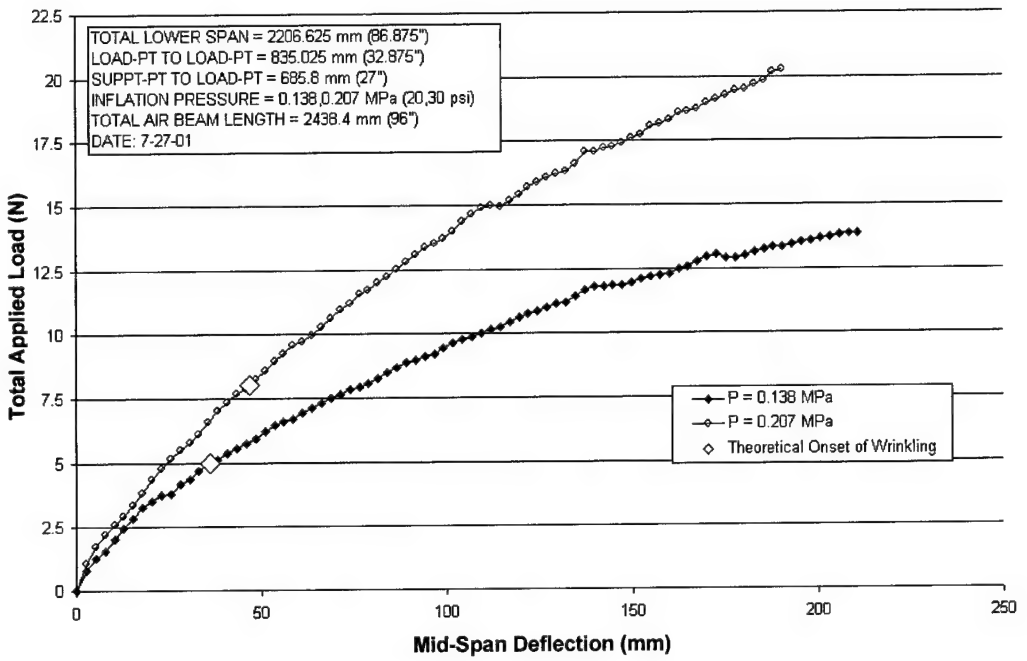

Figure 6. Four-Point-Bend Load-Deflection Curves for Vectran Air Beam at Constant Pressures of 0.138 MPa (20 psi) and 0.207 MPa (30 psi) Using Wide-Span Setup

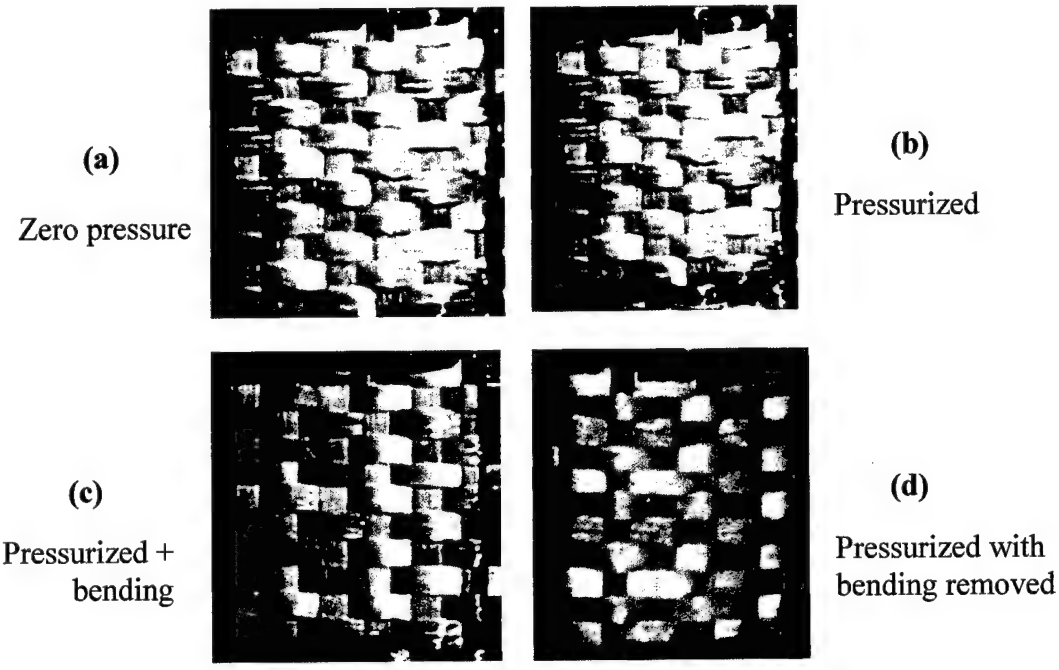

Figure 7. Stages of Fabric Air Beam Deformations

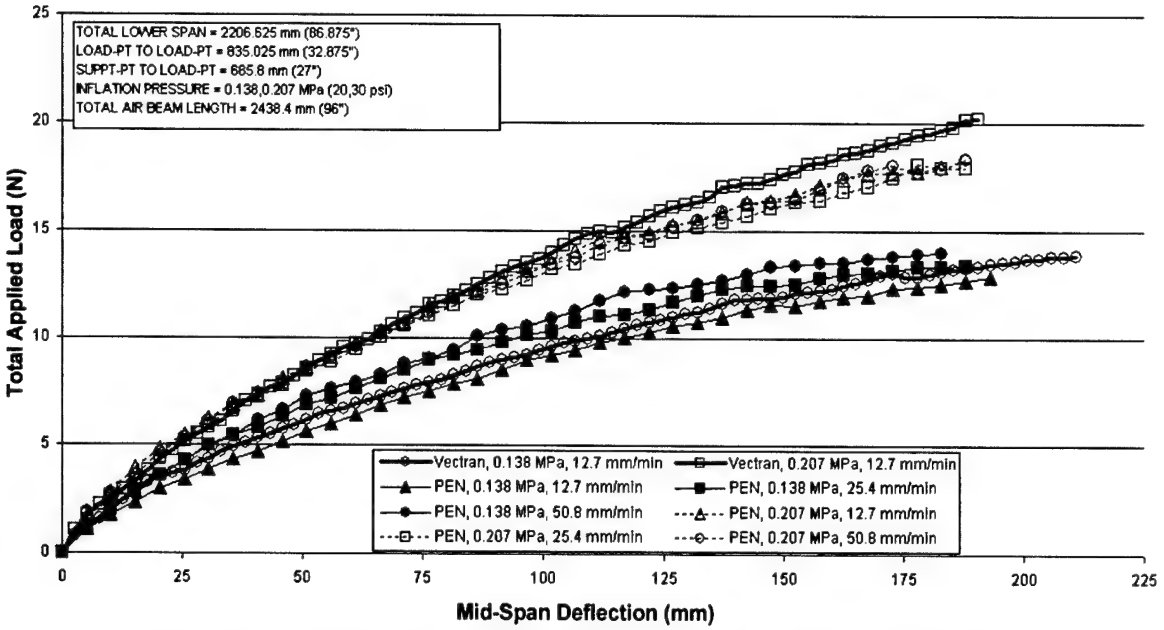

Figure 8. Comparison of Vectran and PEN Air Beams Subjected to Wide-Span, Four-Point Bending

The material properties of the Vectran and PEN tows must be known to accurately model their constitutive impact on the experimental four-point-bend tests. Unlike conventional fabrics, the air beams studied in this research were constructed of tows having zero twist. In a precursory step to the weaving process, twist was removed from the tows, primarily to provide a flatter fabric. In doing so, however, a greater elastic modulus was achieved.

Investigating the strength and the elastic modulus of the tows was accomplished through tensile tests with Instron fiber grips, as shown in figure 9. Sample warp and weft tows were taken from the Vectran and PEN air beams used in the four-point-bend experiments for measurement of their as-woven properties — a necessary step for capturing any fiber property degradation resulting from the weaving process.

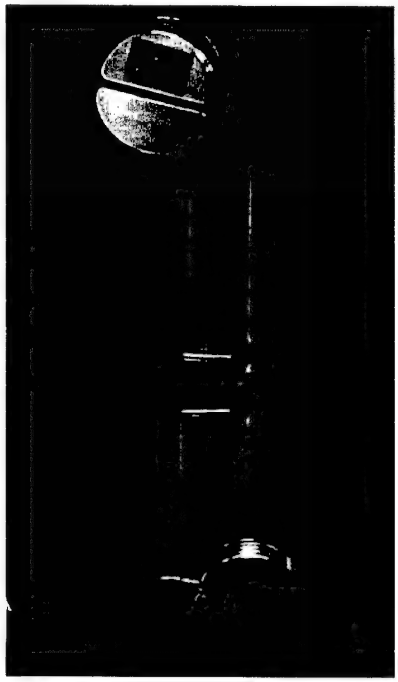

Figure 9. Tensile Tests of Vectran and PEN Tows

ANALYTICAL STRAIN-ENERGY SOLUTION

Contrary to metallic structures, the deflections in the experiments were found to be functions of internal pressure and the shear deformations were observed to be significant. This section simulates the flexure experiment and analytically estimates the effective shear modulus.

Through the derivation of a shear-deformable beam deflection equation, it can be shown that the shear modulus of the fabric is not a function of the tow elastic modulus. With that equation and use of the experimental deflections, the effective in-plane fabric shear modulus G_f is computed, with the equation capturing both the bending and transverse shear deformations that comprise the total mid-span deflection. Although fabric shearing deformations were observed for all flexure tests where inflation pressures ranged from 0.138 to 0.689 MPa (20 to 100 psi), these deformations were observed to decrease with increasing pressure.

The first step of the analytical solution, which involved uncoupling the bending loads from the hoop tows, was based on the assumption that the near-orthogonal tow directions were truly orthogonal, with the warp axis being parallel to the longitudinal axis of the air beam. The warp tows were then taken to exclusively support the bending loads. In a truly orthogonal fabric air beam, the hoop tows can be considered as discrete parallel rings rather than as continuously spiraled tows possessing small lead angles.

In the second step, it was assumed that the discrete tow assembly was a homogeneous, equivalent cylinder with a cross-sectional area equal to the total cross-sectional areas of all the warp tows A_{total}. The inner radius of the equivalent cylinder r_i was taken as the nominal air beam radius, and the outer radius of the equivalent cylinder r_o was computed by

$$r_o = \sqrt{\frac{A_{total}}{\pi} + r_i^2} \quad . \tag{1}$$

Next used was Castigliano's second theorem,[29] which considered the strain energies from both bending and shearing deformations for the equivalent cylinder. The total strain energy, U_{total}, was expressed as

$$U_{total} = \int_0^L \frac{M(x)^2}{2E_{tow}I_{cyl}}\,dx + \int_0^L FS\frac{V(x)^2}{2A_{cyl}G_f}\,dx\,, \tag{2}$$

where

A_{cyl} is the cross-sectional area of the equivalent cylinder (equal to the total area of warp tows (A_{total}),

E_{tow} is the elastic modulus of the warp tow,

FS is the shear strain correction factor (for a tube, this factor is 2.0),

G_f is the pressure-dependent shear modulus of the fabric,

I_{cyl} is the area moment of inertia of the equivalent cylinder,

L is the length of the air beam between support points,

$M(x)$ is the bending moment,

$V(x)$ is the transverse shear force along the axial direction, and

x is the longitudinal position along the length of the beam.

The total mid-span deflection δ_{total} due to the total applied load P_{total} and the displacement wire transducer force Q are derived from minimization of the total strain energy U_{total} with respect to Q (see figure 10), resulting in

$$\delta_{total} = \frac{1}{48}\frac{8a^3P_{total} + 8a^3Q + 6Qac^2 + 12cQa^2 + 12ca^2P_{total} + 3c^2aP_{total} + Qc^3}{E_fI_{cyl}}$$

$$+\frac{1}{4}FS\frac{2aP_{total} + 2aQ + Qc}{G_fA_{cyl}}\,, \tag{3}$$

where a is the distance between the support point and the adjacent load point and c is the distance between the load points.

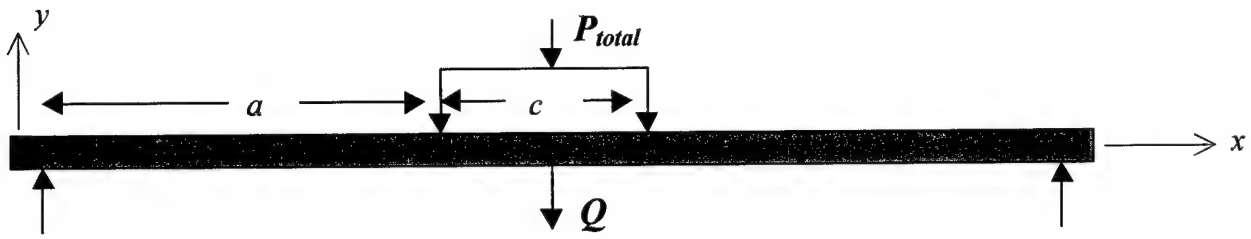

Figure 10. Four-Point-Bend Parameters for Analytical Strain-Energy Solution

The first and second terms of equation (3) represent the bending component δ_{bend} and the shearing component δ_{shear} of the total mid-span deflection, respectively. Use of the second term means that the fabric shear modulus δ_{shear} may be calculated from

$$G_f = \frac{a\left(P_{total} + Q + \frac{Qc}{2a}\right)FS}{2\delta_{shear}A_{cyl}}, \tag{4}$$

indicating that G_f is not a function of the tow elastic modulus E_{tow} and that P_{total} and δ_{shear} are functions of internal pressure.

UNIT-CELL MODELS

The need to develop predictive behavior tools for woven-fabric air beams led to the creation of multiple finite-element models. In each case, Altair HyperMesh 5.0 was used to model the geometry and various versions of HKS ABAQUS were employed to perform the finite-element calculations. Initially, a quarter-symmetry finite-element model of the woven air beam that consisted of the bladder, individual tows, tow contact interactions, and friction was created, with membrane elements also included.

The analysis was extremely time consuming as a result of the numerous contact surfaces, and convergence problems were encountered. The need to obtain a cost-effective, computationally efficient model that would not encounter convergence problems led to the development of a localized tow interaction model of the woven fabric, known as a "unit cell." With this approach,

also called the homogenization method, the effective global material properties of the inflated structure are obtained based on the material properties of the individual tows and their interaction with the contacting orthogonal tows. The technique reduces the number of necessary computations and the run time for full-scale fabric flexure analyses, while it preserves the effects of tow interaction on material behavior.

A unit cell generally consists of several rows of warp and weft tows. In the process of loading an air beam, it was noted that the tows exhibited relative displacement with respect to each other, as shown earlier in figure 7. Figure 11 illustrates two types of kinematic tow interaction modeling methods: (1) rotation only (pinned centers) and (2) rotation and translation. In the rotation-only condition, the centers of the contact areas remain coincident and are hinged, with the friction due only to the relative rotation of the tows (no sliding allowed). This kinematic condition is appropriate for modeling pneumatic muscles, where the tows are braided and the relative angle of rotation is significantly large, as described by Klute and Hannaford.[28] In the rotation and translation condition, there are no kinematic constraints between the two overlapping contact areas, which enables interacting tows to slide and rotate with respect to each other. Therefore, contact-induced friction forces provide resistance to both rotations and translations. The unit-cell modeling in this study considered the second type of contact in which both rotation and translation of the interacting tows occur.

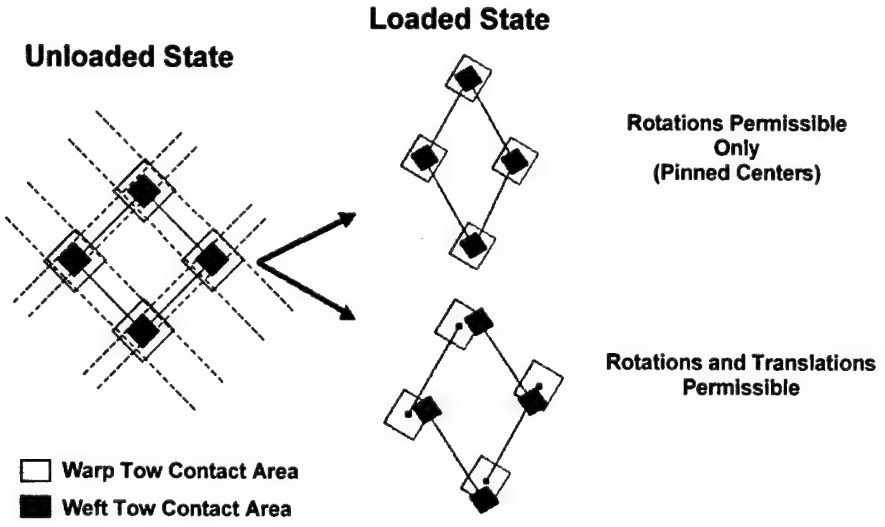

Figure 11. Kinematic Tow Interaction Modeling Methods

The bladder does not contribute any structural stiffness to the fabric, nor is it necessary to include the bladder as a contacting media. Moreover, the inclusion of a bladder contact surface was found to create unnecessary convergence difficulties and to add computational expense. Elimination of the bladder from these models was thus justified.

Three distinct methods for pressurizing the unit-cell models were considered. Shown in figure 12(a), the first option considered the pressure applied only to those regions of the bottom tows lying within the contact areas. However, such loading ignored the pressure on the noncontact areas of the bottom tow. In figure 12(b), the second option addressed the pressure applied to both contacting and noncontacting regions of the tows. Although this distribution represents the full pressure application in the absence of the bladder, it leads to computational difficulties due to "lift off" between orthogonal tows in the overlap regions. The third option, illustrated in figure 12(c), considered the pressure applied to the contacting region and half of the noncontacting region. Even though this choice had associated computational expenses, it was the best representation of the actual inflation pressure and was therefore pursued.

SHELL UNIT-CELL MODEL

It was hypothesized that the elastic and shear moduli of plain-woven fabric structures are highly dependent on internal pressure and, furthermore, that these moduli are independent of one another. A shell unit-cell model was created to show the validity of this assumption.

In the model, each tow was represented by an isotropic thin shell with material properties of either Vectran or PEN, depending on the fabric being studied. Consisting of four warp tows and four weft tows as shown in figure 13(a), the shell unit-cell model was subjected to internal pressures ranging from 0.0138 MPa (1 psi) to 0.276 MPa (40 psi) in a manner consistent with figure 12(c). Contact surfaces and nonlinear slip/stick conditions were employed. Two compliant membrane elements ($E_{membrane} << E_{tow}$) connecting the center points of the central contact regions were created. These membrane elements were used to determine the overall stress and strain of the model and did not contribute to its structural stiffness.

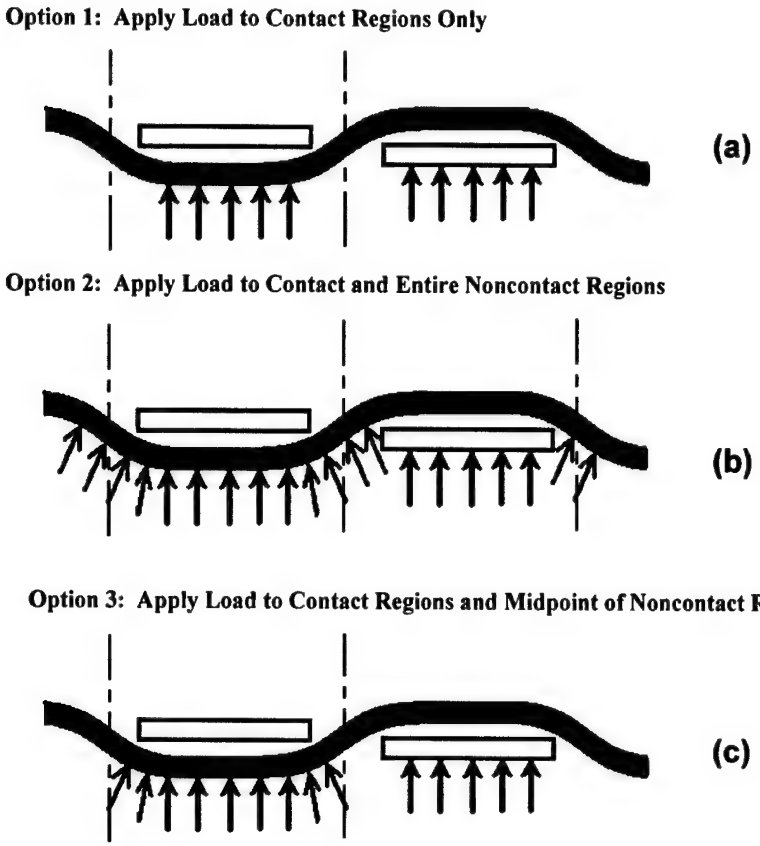

Figure 12. Pressure Application Options for Shell Unit-Cell Model

A three-step computational procedure was employed to determine the elastic and shear moduli of the unit cell. First, as shown in figure 13(a), the warp and weft tows were pressurized.

In the second step, illustrated in figure 13(b), the vertical tows were restrained and the horizontal tows (x-direction) were subjected to +1% displacement. The model was solved, and the stress in the x-direction and the strains in the x- and y-directions were determined. Then, the elastic modulus, $E_1 = \sigma_1/\varepsilon_1$, and Poisson's ratio, $\nu_{12} = -\varepsilon_2/\varepsilon_1$, were calculated.

Next, as part of the second step, the horizontal tows were restrained and the vertical tows (y-direction) were subjected to +1% displacement. The model was solved, and the stress in the y-direction and the strains in the x- and y-directions were determined. The elastic modulus, $E_2 = \sigma_2/\varepsilon_2$, and Poisson's ratio, $\nu_{21} = -\varepsilon_1/\varepsilon_2$, were also computed.

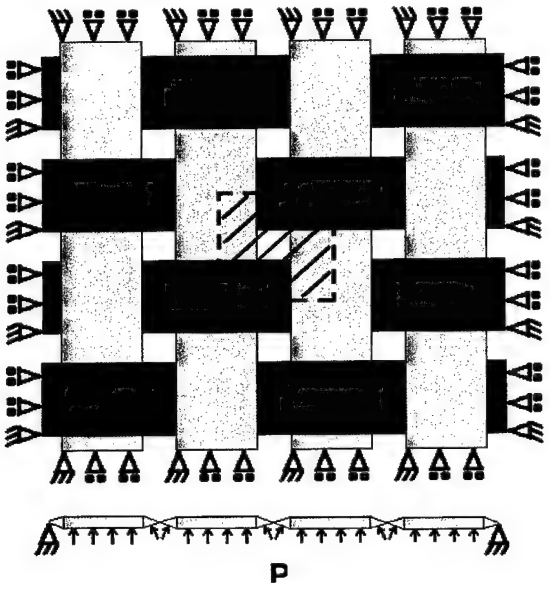

(a) Step 1: Warp and Weft Tows Subjected to Inflation Pressure

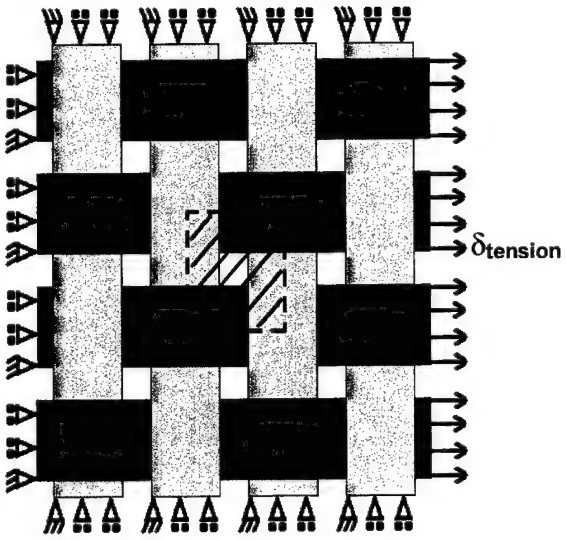

(b) Step 2: Restraint of Vertical Tows and 1% Displacement of Horizontal Tows

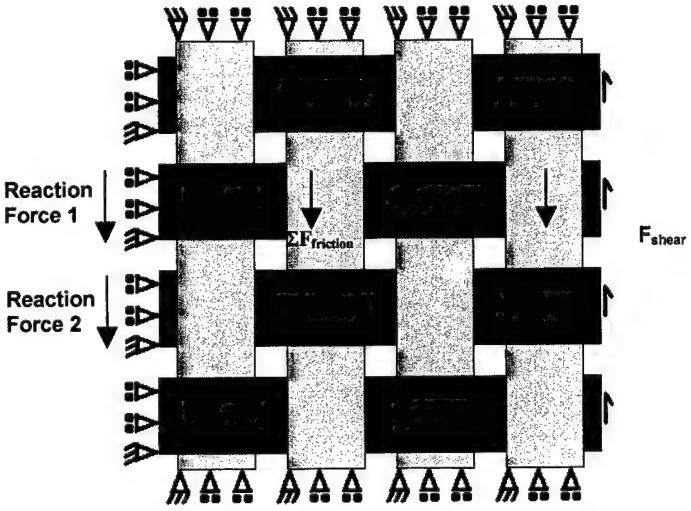

(c) Step 3: Horizontal Tow Subjected to Shear Force

Figure 13. Shell Unit-Cell Model

In the third step, the following two approaches were used to calculate shear modulus G_{12} (or G_f) to illustrate its independence from the elastic moduli. The first technique assumed that the fabric was a continuum with orthotropic material properties. The unit-cell model in this case was subjected to the +1% nodal displacement at a 45° angle. The finite-element model was solved, and the stress and strain of the unit-cell model at the 45° angle were determined. The shear modulus was calculated according to Jones[30] by

$$G_f = \left(4/E_x - 1/E_1 - 1/E_2 + 2\upsilon_{12}/E_1\right)^{-1}, \tag{5}$$

where E_x is the elastic modulus in the direction of the 45° load. This expression may be appropriate for fabrics with stiff coatings.

The second technique for calculating G_f assumed that the woven fabric was not a continuum and that each tow independently responded to the external load. In this case, the horizontal tows were subjected to a shear force F_{shear}, as shown in figure 13(c). The shear modulus was then calculated based on the equilibrium of the horizontal tow and its shear deformation as

$$G_f = G_{12} = \tau_{shear}/\gamma, \tag{6}$$

with

$$\tau_{shear} = \Sigma F_{reaction}/\Sigma A \tag{7}$$

and

$$\gamma = \arctan(\delta_{shear}/L), \tag{8}$$

where $\Sigma F_{reaction}$ is the sum of reaction forces at the support, δ_{shear} is the nodal transverse displacement, A is the tow cross section, and L is the tow length.

A number of tests were performed in which the coefficient of friction was varied and the changes in the elastic and shear moduli were determined. The results of the shell unit-cell model tests were therefore parametric in both friction and pressure.

BEAM-ELEMENT UNIT-CELL MODEL

The warp and weft tows consist of many unidirectional fibers aligned with zero twist, as seen earlier in figure 2. This tow structure leads to transverse elastic tow moduli (E_2 and E_3) equal to zero. If the spacing between adjacent axial tows or between adjacent hoop tows is on the order of the magnitude of the tow width, then it was hypothesized that the internal pressure would expand the bladder into the spacing and apply a lateral load to the tows. Transversely loading the tow with a negligible E_2 would cause necking of the tow structure, as illustrated in figure 14.

Because tows that are comprised of shell elements exhibit undesired transverse stiffnesses that do not allow tow necking under the loading described, it is preferable in a fabric with wide-weave spacing to model the tow as a series of beam or cable elements. It was hypothesized that such a model would eliminate the artificial transverse stiffening associated with shell elements, thus permitting tow necking. To demonstrate the validity of this hypothesis, a model was created in which a single tow was represented as a collection of independent, unidirectional fibers using beam elements. Transferring the pressure to the beam elements was accomplished by modeling the bladder with compliant shell elements. Confirmation of the tow-necking hypothesis is observed in figure 15.

Having shown that tows composed of beam elements demonstrated the desired behavior, it was now important to simulate the interaction of two contacting tows. Two sets of orthogonal tows and a bladder, modeled as beam elements and shell elements, respectively, were created. The ABAQUS solver, however, did not permit beam-to-beam contact. Therefore, compliant membrane elements (which did not contribute structurally to the model) were created between the beam elements of each tow to capture the tow-to-tow contact kinematics. This tow interaction model is shown in figure 16, where it is demonstrated (1) that contact between tows represented as beam elements can be effectively employed and (2) that the presence of as few as two orthogonal tows significantly decreases the amount of tow-necking deformation.

Next, a beam unit-cell model was developed based on this same method for creating tow-to-tow contact. The model represented the weave spacing of the actual air beams and consisted of two warp (axial) tows and two weft (hoop) tows. Each tow was comprised of 14 fibers of 0.1-mm diameter (see figure 17). The fibers were modeled at their centerlines and placed next to one

Pre-Inflation

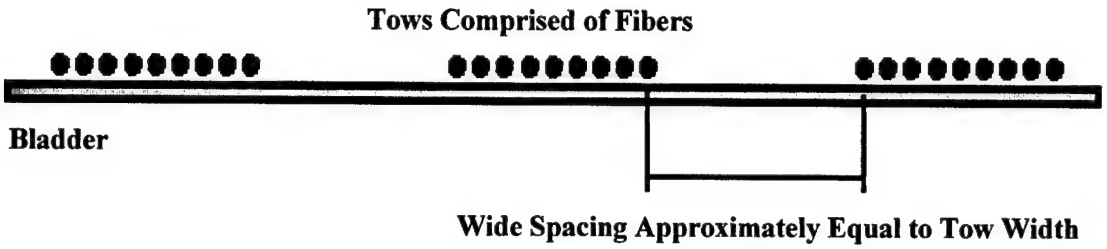

Post-Inflation

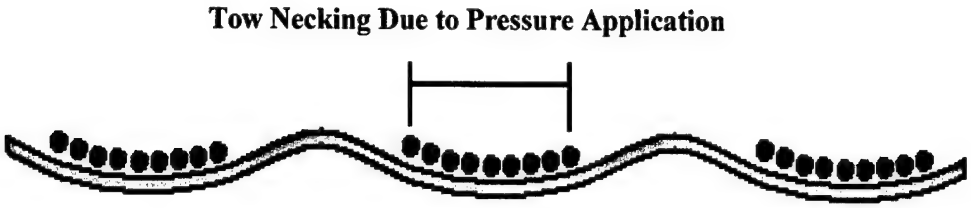

Figure 14. Hypothesized Bladder/Tow Interaction for Large-Weave Spacing

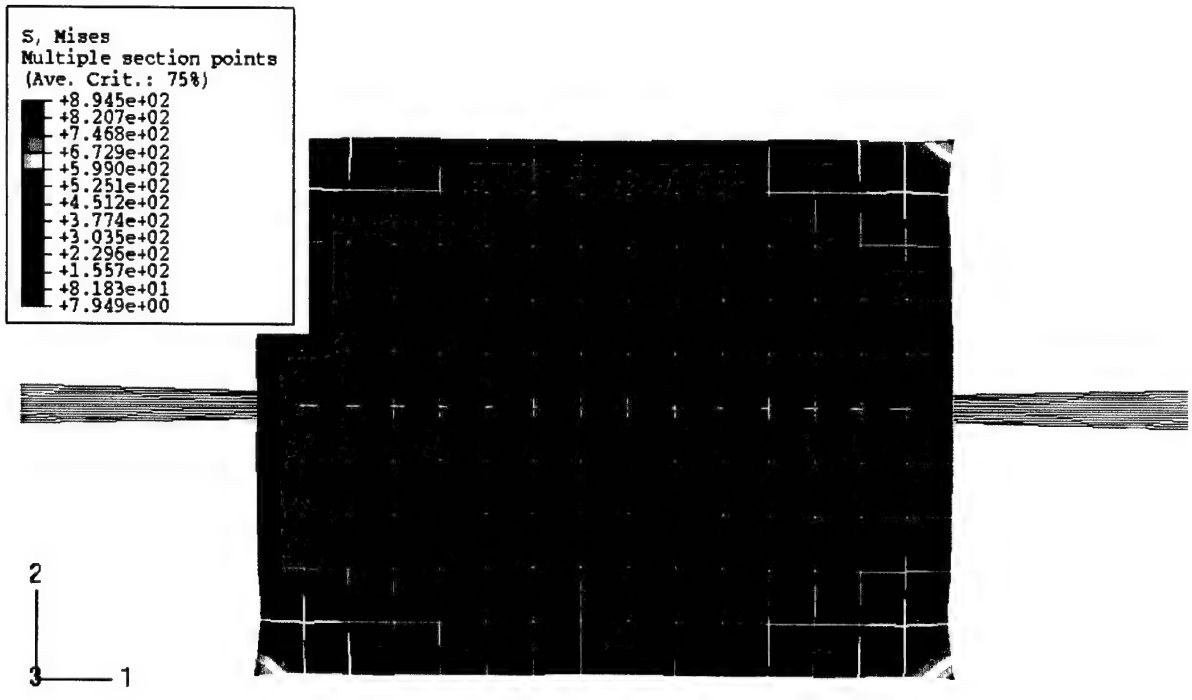

Figure 15. Tow Necking in Beam-Element Model

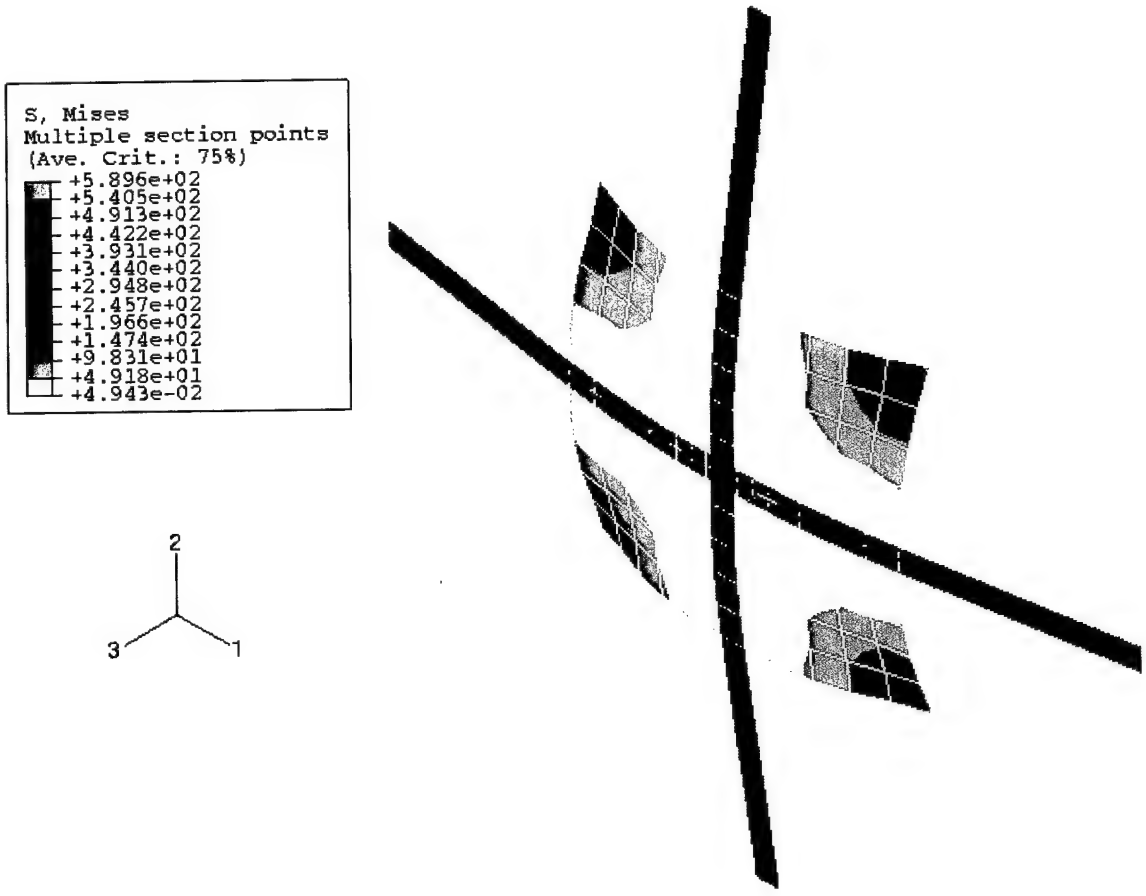

Figure 16. Orthogonal Beam-Element Tow Interaction Model

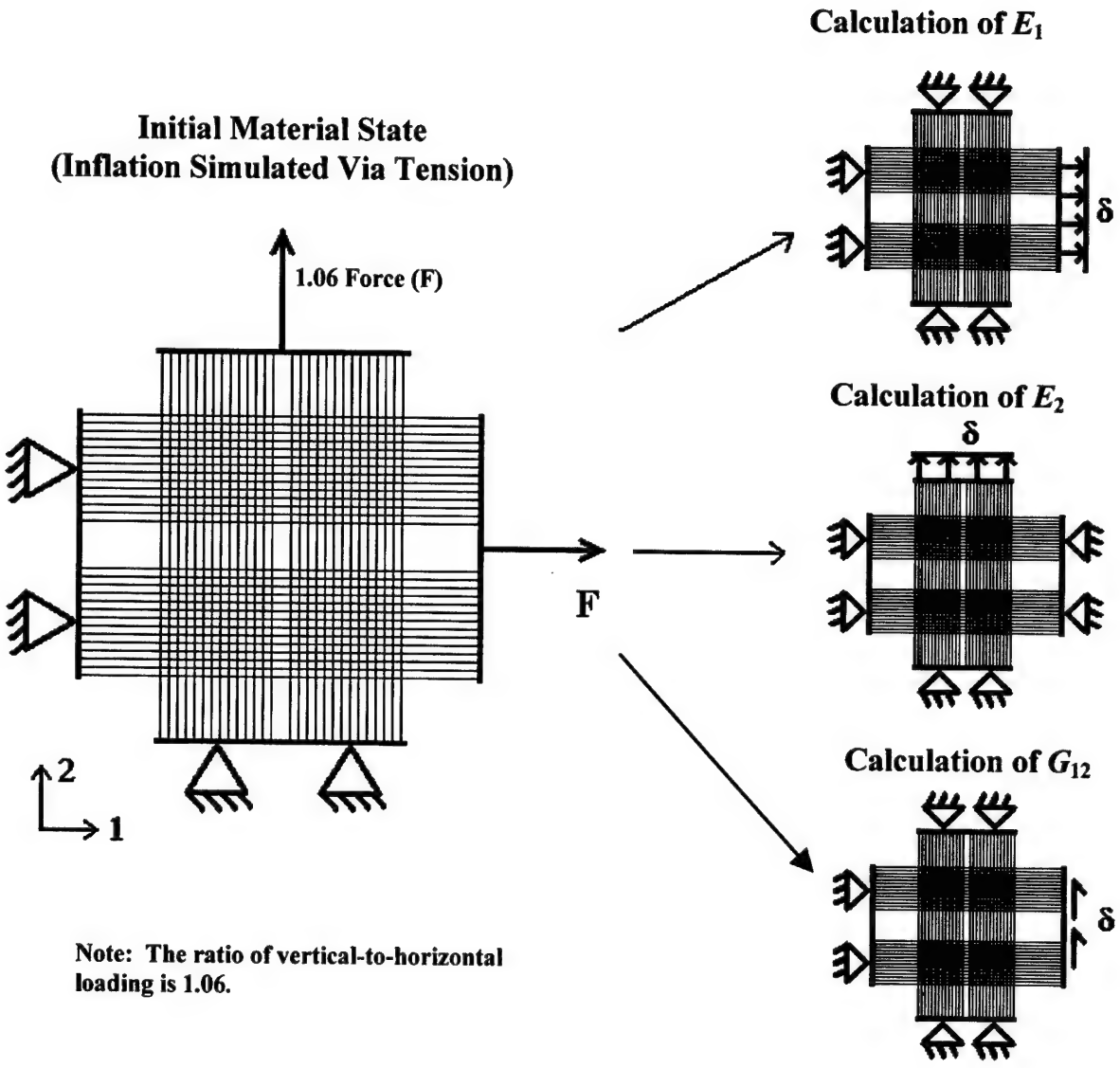

Figure 17. Beam-Element Unit-Cell Model

another such that the centerline distances were 0.1 mm. The two weft tows were separated by 0.15 mm, and the two warp tows by 1.1 mm. These values were derived from measurements of the 50.8-mm (2.0-inch) diameter air beams used in the experiments. The coefficient of friction μ between the overlapping beam elements was considered to be 0.5 based on the results of the shell unit-cell model. To ensure the removal of boundary-induced end effects, the beam lengths were extended. While the use of membrane elements for the bladder appeared to be the optimal choice for the beam unit-cell model, computational difficulties and nonconvergence issues arose when internal pressure was applied. Eliminating the bladder required that each fiber (beam element) be subjected to an equivalent pre-tension force corresponding to the internal pressure, which was calculated as described below.

First, it is assumed that N_a is the total number of tows in the warp (axial) direction, n_h is the number of tows per unit length in the weft (hoop) direction, and A_t is the cross-sectional area of the tow. If the internal pressure of the air beam is p and the mean diameter is d, then, through static equilibrium, the stresses in the hoop tows σ_h and in the axial tows σ_a are

$$\sigma_h = pd/(2A_t n_h) \tag{9}$$

and

$$\sigma_a = \pi pd^2/(4A_t n_a) \ , \tag{10}$$

and the ratio of hoop-to-axial tow stress is

$$\sigma_h/\sigma_a = 2N_a/\pi d n_h \ . \tag{11}$$

The values of N_a and n_h were 63 and 19, respectively, with substitution leading to $\sigma_h/\sigma_a = 1.06$. In fact, air beam designers generally choose the number of warp and weft tows such that the tensions in the axial and hoop tows are nearly equal. This approach ensures equal factors of safety in both the warp and weft directions against fabric burst failures.

The above discussion has shown that the beam-element unit-cell model was initially subjected to the pre-tension force corresponding to the internal pressure so that the bladder could be eliminated.

To determine the elastic and shear moduli of the beam-element unit-cell model, three analytical experiments similar to those for the shell unit-cell model were performed. First, the vertical tows of the model were constrained in the y-direction and the horizontal tows were subjected to +1% strain in the x-direction. Next, the horizontal tows were constrained in the x-direction and the vertical tows were subjected to +1% in the y-direction. Lastly, the vertical tows were constrained and the horizontal tows were subjected to the +1% shear strain in the y-direction.

FINITE-ELEMENT MODEL

A global, quarter-symmetry finite-element model of the four-point-bending experiment was created. The supports were modeled as rigid bodies defined to be in frictionless contact with the air beam. The support and load points were allowed to rotate in a manner similar to the saddles used in the four-point-bending experiments, but were otherwise constrained in all other translations and rotations. To load the air beam, the two load points were displaced downward toward the beam. The model consisted of 3236 shell elements, each with a 0.1-mm thickness.

The elastic and shear moduli of the beam unit-cell model were employed as the material properties of the shell elements in the global model. Although nine elastic material constants (E_1, E_2, E_3, ν_{12}, ν_{13}, ν_{23}, G_{12}, G_{13}, and G_{23}) were required, only E_1, E_2, and G_{12} had been calculated from the beam unit-cell model. Because a thin-shell formulation was used, the elastic modulus E_3 did not influence the global beam deflection and was therefore chosen to be of the same order of magnitude as E_1 and E_2 (i.e., E_3 = 64,000 MPa).

It was also noted that any load applied in the direction of one tow was decoupled from all orthogonal tows. Because such a situation infers that Poisson's ratio is nearly 0, the condition where $\nu_{12} = \nu_{13} = \nu_{23} = 0.0$ was applied. No method was developed to determine G_{13} and G_{23}, as it was hypothesized that neither value had a significant effect on the beam deflection. In support of this hypothesis, the values of G_{13} and G_{23} were assumed to be equal and a parametric study was performed in which the values were varied and the beam deflections compared.

RESULTS

Material properties of Vectran and PEN tows were measured in a simple tension experiment during which the crosshead displacement rate of an Instron machine was set to 12.7, 25.4, and 50.8 mm/minute (0.5, 1.0, and 2.0 inches/minute). The samples of the warp and weft tows used in the study were taken from previously tested Vectran and PEN air beams.

Determinations of the maximum stress, strain, and the average elastic modulus are presented in table 1. Note that figure 18 shows the average elastic modulus of Vectran and PEN tows increasing as the crosshead speed is increased. It was observed that the elastic modulus of the weft (hoop) tows was 25% less than that of warp (axial) tows.

From the analytical strain-energy solution, the equivalent in-plane fabric shear modulus, G_f, for the 50.8-mm (2.0-inch) diameter Vectran beam pressurized to 0.689 MPa (100 psi) was calculated as 86.06 MPa (12,480 psi). The computed bending and shear components of the mid-span deflection were 12.39 mm (0.488 inch) and 39.54 mm (1.557 inches), respectively, which resulted in a shear-to-bending deflection ratio of 3.1 to 1.0, which was observed to decrease with increasing pressures. It is clear that the shear deformation dominated the flexural behavior of the air beam. In conventional metal structures, shear deformation is usually negligible.

The coefficient of friction was varied in the shell unit-cell model, and the changes in the elastic and shear moduli (E_1, E_2, and $G_f = G_{12}$) were determined as a function of the internal pressure (see figures 19–21). When the coefficient of friction was changed from 0.0 to 0.5, it was observed that the increase does not significantly impact the elastic and shear moduli. Figures 19 and 20 also indicate that the changes in the elastic moduli, E_1 and E_2, with respect to pressure are similar.

The elastic and shear moduli in the beam unit-cell model were calculated for an internal pressure of 0.138 MPa (20 psi), resulting in $E_1 = 64{,}033$ MPa, $E_2 = 64{,}098$ MPa, and $G_f = G_{12} = 60.96$ MPa. Similarly, for an internal pressure of 0.207 MPa (30 psi), the elastic moduli were calculated as $E_1 = 64{,}045$ MPa, $E_2 = 64{,}049$ MPa, and $G_f = G_{12} = 80.64$ MPa.

Table 1. Tensile Properties of As-Woven Vectran and PEN Tows

Vectran							
1500 Denier	300 Filaments	Filament Diameter = 0.00090551				Tow Cross-Sectional Area (in.^{2}) = 0.0001932	
Test #	Vectran 1500 Fiber Type	Crosshead Rate (ipm)	Maximum Load (lb)	Maximum Stress (psi)	Maximum Strain (in./in.)	Maximum Strain (%)	Modulus (psi)
1	Axial	0.5	52.0	269,156	0.023	2.3	11,702,432
2	Axial	0.5	51.2	265,015	0.025	2.5	10,600,603
3	Axial	0.5	54.3	281,061	0.024	2.4	11,710,871
		AVERAGES------>	**52.5**	**271,744**	**0.024**	**2.4**	**11,337,969**
7	Axial	1.0	50.5	261,392	0.020	2.0	13,069,591
8	Axial	1.0	50.0	258,804	0.021	2.1	12,323,990
9	Axial	1.0	51.3	265,533	0.023	2.3	11,544,899
		AVERAGES------>	**50.6**	**261,909**	**0.021**	**2.1**	**12,312,827**
16	Axial	2.0	63.8	330,234	0.022	2.2	15,010,620
17	Axial	2.0	63.0	326,093	0.026	2.6	12,542,030
18	Axial	2.0	59.9	310,047	0.021	2.1	14,764,140
		AVERAGES------>	**62.2**	**322,124**	**0.023**	**2.3**	**14,105,596**
4	Hoop	0.5	69.8	361,290	0.028	2.8	12,903,217
5	Hoop	0.5	65.6	339,551	0.030	3.0	11,318,352
10	Hoop	0.5	52.0	269,156	0.027	2.7	9,968,739
		AVERAGES------>	**62.5**	**323,332**	**0.028**	**2.8**	**11,396,769**
6	Hoop	1.0	65.3	337,998	0.027	2.7	12,518,435
11	Hoop	1.0	70.0	362,325	0.026	2.6	13,935,589
12	Hoop	1.0	56.3	291,413	0.029	2.9	10,048,726
		AVERAGES------>	**63.9**	**330,579**	**0.027**	**2.7**	**12,167,583**
13	Hoop	2.0	68.3	353,526	0.023	2.3	15,370,695
14	Hoop	2.0	76.6	396,487	0.030	3.0	13,216,247
15	Hoop	2.0	73.0	377,854	0.025	2.5	15,114,141
		AVERAGES------>	**72.6**	**375,956**	**0.026**	**2.6**	**14,567,028**

PEN							
1500 Denier	300 Filaments	Filament Diameter = 0.00090551				Tow Cross-Sectional Area (in.^{2}) = 0.0001932	
Test #	PEN 1500 Fiber Type	Crosshead Rate (ipm)	Maximum Load (lb)	Maximum Stress (psi)	Maximum Strain (in./in.)	Maximum Strain (%)	Modulus (psi)
1	Axial	0.5	17.8	92,134	0.038	3.8	2,424,583
2	Axial	1.0	17.6	91,099	0.040	4.0	2,277,473
3	Axial	2.0	19.2	99,381	0.038	3.8	2,615,280
		AVERAGES------>	**18.2**	**94,205**	**0.039**	**3.9**	**2,439,112**

The beam unit-cell model material properties were then implemented in a quarter-symmetry four-point-bend model. A typical shear stress field of the deformed quarter-symmetry finite-element model at 0.138 MPa (20 psi) is shown in figure 22. The analysis was performed as a parametric study that compared the load-deflection curves of the air beam for various G_{13} and G_{23} values ($G_{13} = G_{23}$), with results as shown in figure 23. As can be seen in this figure, the effects of increasing the transverse shear moduli G_{13} and G_{23} are minimal.

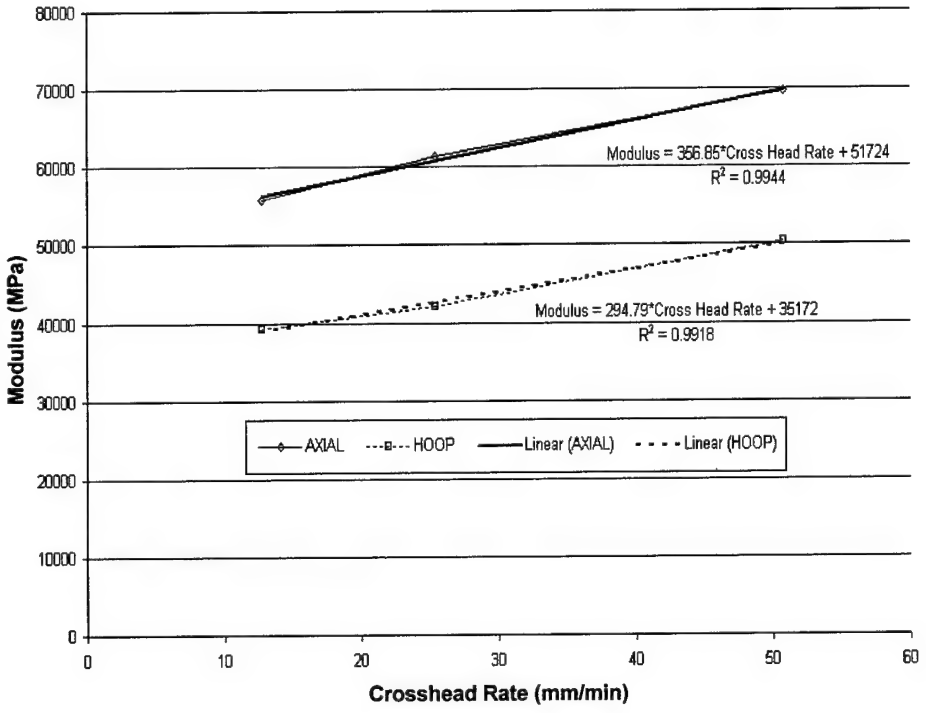

Figure 18. Rate-Dependent Elastic Modulus of As-Woven Vectran Warp and Weft Tows

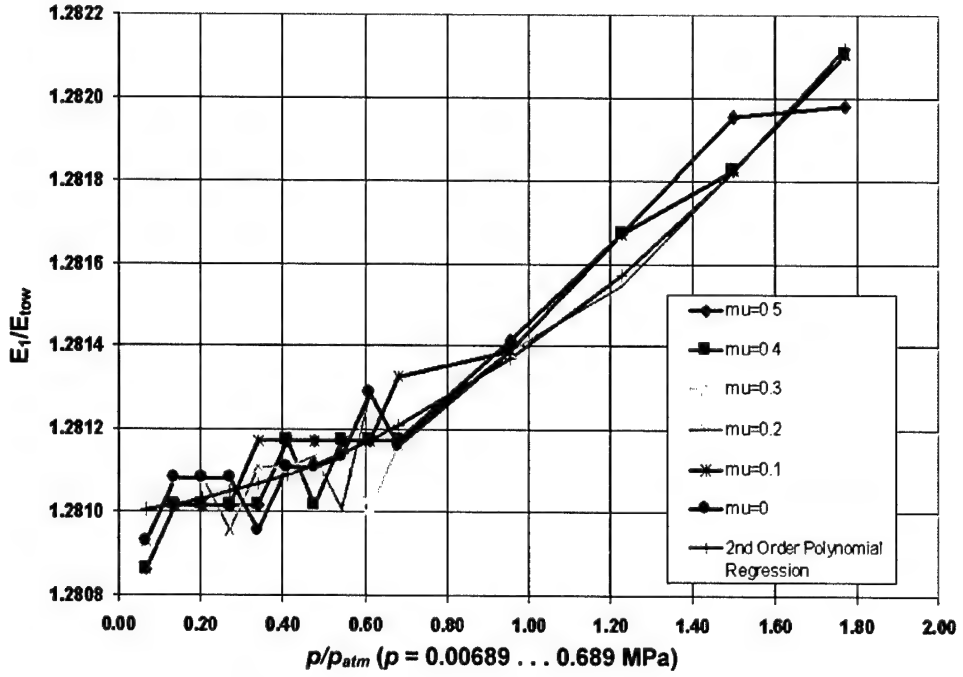

Figure 19. Nondimensionalized Plot of Fabric Modulus (E_1) Versus Pressure for Various Coefficients of Friction

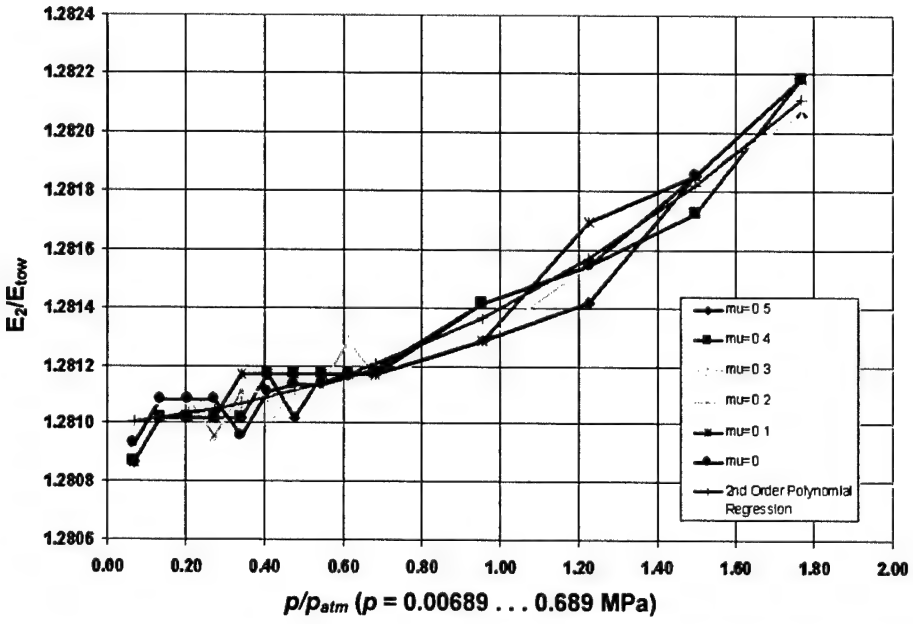

Figure 20. Nondimensionalized Plot of Fabric Modulus (E_2) Versus Pressure for Various Coefficients of Friction

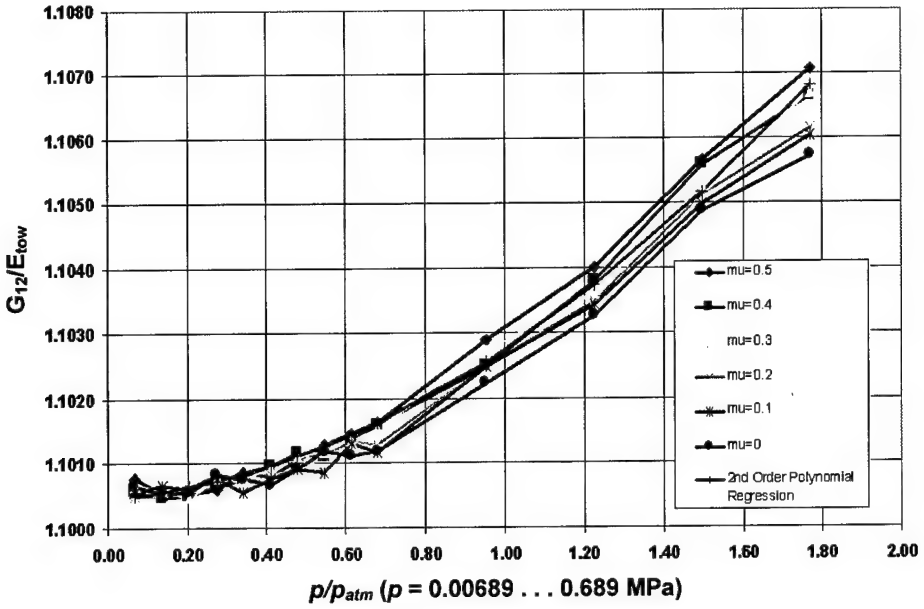

Figure 21. Nondimensionalized Plot of Fabric Shear Modulus ($G_f = G_{12}$) Versus Pressure for Various Coefficients of Friction

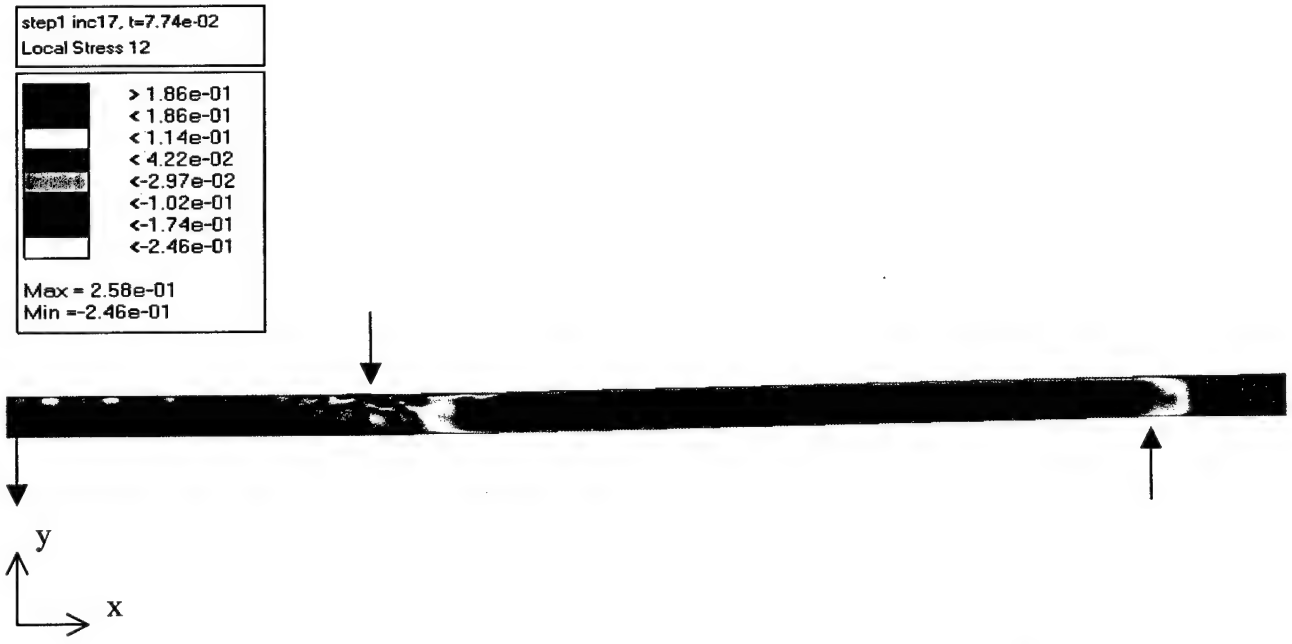

Figure 22. Contour Plot of Shear Stress (τ_{12}) for Quarter-Symmetry, Four-Point-Bend Finite-Element Model

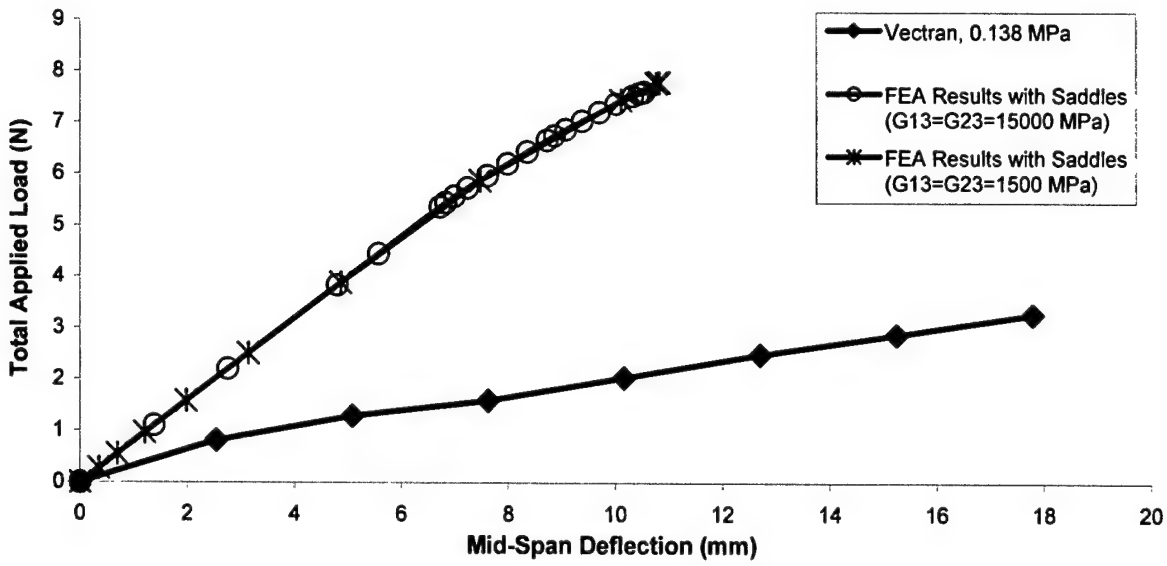

Figure 23. Comparison of Results from Four-Point-Bend Finite-Element Shell Model to Experimental Results for 50.8-mm (2.0-Inch) Diameter Vectran Air Beam at 0.138 MPa (20 psi)

CONCLUSIONS

It was observed that a complete model of the air beam, including each warp and weft tow and all tow-to-tow contact surface interactions, was not computationally possible. To study both the micromechanics and macromechanics of pressurized-fabric air beams, a four-point-bend experimental setup was designed and manufactured for the testing of six 50.8-mm (2.0-inch) diameter Vectran and PEN air beams from Federal Fabrics-Fibers Inc.*

When the air beam mid-span deflections were measured as functions of pressure and external load, it was observed that tow slippage and fabric-shearing deformations occurred. In a separate experiment, the as-woven elastic modulus of both Vectran and PEN tows was measured.

Tensile tests of the individual Vectran and PEN tows showed increasing elastic moduli as the load rate increased, with the ratio of as-woven Vectran-to-PEN tow moduli being 4.7 to 1.0. It is important to note that the Vectran and PEN air beams exhibited similar deflections under

*The highly compliant bladder was considered to be nonstructural because it did not contribute to the stiffness of the air beams.

identical loads. Thus, the tow elastic modulus did not significantly affect the deflection of the air beam for the pressures and loads considered.

The strain-energy-based closed-form solution of the four-point-bend experiment was developed. An equation for the mid-span deflection of the air beam was derived that included both bending and shear deformation components. It was concluded that the shear component was approximately 3.1 times greater than the bending component for an inflation pressure of 0.689 MPa (100 psi).

Micromechanical tow models representing the unit cell of the air beam fabric were analyzed. The shell unit-cell model represented the tow as thin-shell elements, while the beam unit-cell model represented the tow as sets of parallel beam elements.

The shell unit-cell model was the first attempt to validate the hypothesis that the shear modulus of a plain-woven fabric structure is dependent on internal pressure and is independent of the elastic moduli. In addition, this model was used to establish the influence of the internal pressure, weave geometry, and coefficient of friction on the effective elastic and shear moduli. It was found that the elastic and shear moduli increase as the internal pressure increases — that is, the structure becomes stiffer in extension and bending with increasing pressure. Moreover, results showing small displacements for the interacting tows relative to tow width indicated that the coefficient of friction between the tows did not influence the elastic and shear moduli.

The beam unit-cell model, which provided a more realistic simulation of the tows, was used to determine the elastic and shear moduli of the fabric.

The material properties of the localized unit cell were then used for the global model of a simply supported, inflated air beam subjected to four-point flexure loading. The load and support points were modeled as saddles to be representative of the experimental setup. Contact surfaces were defined for each saddle and along the air beam regions in contact with the saddles. The global finite-element model results, shown in figure 23, are stiffer than those of the experiment. This condition is due to the variations that occur in air beam material properties during loading. More specifically, it was found that the material properties are dependent upon weave density and tow spacing. In direct relation to the change in tow tension, the tow spacing

varied with loading, increasing on the tensile region of the air beam and decreasing on the compressive region. As a consequence, during the four-point-bend experiments, the elastic and shear moduli of the fabric decreased on the compressive side and increased on the tensile side. However, because the finite-element model employed constant elastic and shear moduli throughout the full loading event, the observed bending behavior was materially nonlinear with respect to both pressure and applied loading.

Curves representing the variations in elastic and shear moduli relative to pressure and the coefficient of friction have been generated. It was shown that the air beam deflection is a function of the internal pressure and bending loads. In addition, the fabric elastic modulus was found to be pressure dependent and slightly greater than the modulus of the tow (although it was decided that the use of a tow with a higher elastic modulus will not significantly influence the deflection of the air beam at a given pressure). Furthermore, it was concluded that air beams coated with neoprene/urethane can carry approximately twice the load of uncoated beams for the same deflection.

This research has shown that pneumatic or pressurized tube structures differ fundamentally from conventional metal and fiber/matrix composite structures. While the plain-woven fabric appeared to be an orthotropic material, its mechanical behavior indicated otherwise. That is, the fabric did not behave as a continuum, but rather behaved as a discrete assemblage of individual tows whose effective material properties depended upon the internal pressure of the beam, the weave geometry, and the contact area of interacting tows.

REFERENCES

1. Private notes from G. Brown, Vertigo Inc., Lake Elsinore, CA, 2001.

2. M. Stein and J. M. Hedgepeth, "Analysis of Partially Wrinkled Membranes," NASA Technical Note D-813, National Aeronautics and Space Administration, Washington, DC, 1961.

3. W. B. Fichter, "A Theory for Inflated Thin-Wall Cylindrical Beams," NASA Technical Note D-3466, National Aeronautics and Space Administration, Washington, DC, 1966.

4. P. S. Bulson, "Design Principles of Pneumatic Structures," *The Structural Engineer*, vol. 51, no. 6, June 1973.

5. E. C. Steeves, "Fabrication and Testing of Pressurized Rib Tents," Technical Report 79-008, United States Army, Soldier Biological Chemical Command, Natick, MA, 1979.

6. E. C. Steeves, "The Structural Behavior of Pressure Stabilized Arches," Technical Report 78/018 (AD-A063263), United States Army, Soldier Biological Chemical Command, Natick, MA, 1978.

7. E. C. Steeves, "Behavior of Pressure Stabilized Beams Under Load," Technical Report 75-47-AMEL, United States Army, Soldier Biological Chemical Command, Natick, MA, 1975.

8. E. C. Steeves, "A Linear Analysis of the Deformation of Pressure Stabilized Beams," Technical Report AND-006-493, United States Army, Soldier Biological Chemical Command, Natick, MA, 1975.

9. E. C. Steeves, "Pressure Stabilized Beam Finite Element," Technical Report 79-002, United States Army, Soldier Biological Chemical Command, Natick, MA, 1978.

10. M. Tarfaoui and S. Akesbi, "A Finite Element Model of Mechanical Properties of Plain Weave Collides and Surfaces," *A: Physicochemical and Engineering Aspect Journal*, vol. 187-188, 2001, pp. 439-448.

11. L. Bejan and V. F. Poterasu, "Woven Composite Material Design by Orthotropic Compliance Averaging Method Using Mathematica," *Computer Methods in Applied Mechanics and Engineering*, vol. 179, nos. 1-2, 1999, pp. 53-65.

12. P. H. Vandeurzen, J. Ivens, and I. Verpoest, "A Three-Dimensional Micromechanical Analysis of Woven-Fabric Composite: II Elastic Analysis," *Journal of Composite Science and Technology*, vol. 56, no. 11, 1996, pp. 1317-1327.

13. K. Woo and J. Whitcomb, "Global/Local Finite Element Analysis for Textile Composites," *Journal of Composite Materials*, vol. 33, no. 16, 1994, pp. 1305-1321.

14. K. Woo, "Three-Dimensional Failure Analysis of Plain Weave Textile Composite Using a Global/Local Finite Element Method," *Journal of Composite Materials*, 1996, vol. 30, pp. 985-1003.

15. J. L. Kuhn and P. G. Charalambides, "Modeling of Plain Weave Fabric Composite Geometry," *Journal of Composite Materials*, vol. 33, no. 3, 1999, pp. 188-220.

16. J. L. Kuhn, S. I. Hann, and P. G. Charalambides, "A Semi-Analytical Method for the Calculation of the Elastic Micro-Fields in Plain Weave Fabric Composites Subjected to In-Plane Loading," *Journal of Composite Materials*, vol. 33, no. 3, 1999, pp. 221-256.

17. X. Ruan and T. W. Chou, "Failure Behavior of Knitted Fabric Composites," *Journal of Composite Materials*, vol. 32, no. 3, 1998, pp. 198-222.

18. H. T. Hahn and R. Pandey, "A Micromechanics Model for Thermoelastic Properties of Plain Weave Fabric Composites," *Journal of Engineering Materials and Technology*, vol. 116, 1994, pp. 517-523.

19. S. Li, J. S. Tsai, and L. J. Lee, "Preforming Analysis of Biaxial Braided Fabric Sleeving on Pipes and Ducts," *Journal of Composite Materials*, vol. 34, no. 6, 2000, pp. 479-501.

20. T. L. Norman, P. Allison, J. W. Baldwin, B. K. Gracias, and D. Seesdorf, "Effect of Tow Alignment on the Mechanical Performance of 3D Woven Textile Composites," *Composite Manufacturing*, vol. 4, 1993, pp. 209-215.

21. T. H. Ueng and K. B. Cheng, "Friction Core-Spun Yarns for Electrical Properties of Woven Fabrics," *Composites Part A: Applied Science and Manufacturing*, vol. 32, no. 10, 2001, pp. 1491-1496.

22. T. C. Lim, S. Ramakrishna, and H. M. Shang, "Optimization of the Formability of Knitted Fabric Composite Sheets by Means of Combined Deep Drawing and Stretch Forming," *Journal of Materials Processing Technology*, vol. 89-90, 1999, pp. 99-103.

23. M. P. Flanagan and M. A. Zikry, "An Experimental Investigation of High Velocity Impact and Penetration Failure Modes in Textile Composites," *Journal of Composite Materials*, vol. 33, no. 12, 1999, pp. 1080-1103.

24. Y. P. Siow and V. P. W. Shim, "An Experimental Study of Low Velocity Impact Damage in Woven Fiber Composites," *Journal of Composite Materials*, vol. 32, no. 12, 1998, pp. 1178-1201.

25. S. Warner, *Fiber Science*, Prentice Hall, Princeton, NJ, 1995.

26. F. Otto, *Tensile Structures*, MIT Publications, Massachusetts Institute of Technology, Cambridge, MA, 1962.

27. R. H. Plaut, J. K. S. Goh, M. Kigudde, and C. D. Hammerand, "Shell Analysis of an Inflatable Arch Subjected to Snow and Wind Loading," *International Journal of Solids and Structures*, vol. 37, no. 31, 2000, pp. 4275-4288.

28. K. G. Klute and B. Hannaford, "Finite Element Modeling of McKibben Artificial Muscle Actuators," *IEEE/ASME Transactions on Mechatronics*, March 1998.

29. A. C. Ugural and S. K. Fenster, *Advanced Strength and Applied Elasticity*, second edition, Elsevier North-Holland Publishing Company, New York, 1977.

30. R. Jones, *Mechanics of Composite Materials*, Hemisphere Publishing Corporation, NewYork, 1975.

INITIAL DISTRIBUTION LIST

Addressee	No. of Copies
U.S. Army Soldier Biological Chemical Command, Natick, MA (J. Hampel, F. Kostka, C. Quigley, T. Godfrey, A. Murphy, M. Jee, R. Benney, G. Thibault, J. Miletti, G. Gildea)	10
Army Research Laboratory – Vehicle Structures Directorate, Hampton, VA (A. Johnson)	1
Army Research Laboratory, Weapons and Materials Research Directorate, Aberdeen Proving Ground, MD (D. Granville, R. Dooley)	2
Army Corps of Engineers, Engineer Research and Development Center, Vicksburg, MS (D. Resio, J. Fowler, J. Melby)	3
Army Research Office, Research Triangle Park, NC (G. Anderson, A. Rajendran, B. LaMattina)	3
Office of Naval Research, Arlington, VA (ONR 334 – R. Barsoum)	1
Defense Technical Information Center	2
Center for Naval Analyses	1
The City College of New York, NY (A. M. Sadegh)	5
Northeastern University, Boston, MA (J. Rossettos)	1
Federal Fabrics-Fibers Inc., Lowell, MA (Z. Horovitz, F. Geurts)	2
Vertigo Inc., Lake Elsinore, CA (G. Brown)	1